Computers and Mathematics with Applications 193 (2025) 132–156

Contents lists available at ScienceDirect

Computers and Mathematics with Applications

journal homepage: www.elsevier.com/locate/camwa

Constrained maximization of conformal capacity

Harri Hakula [a,*,1], Mohamed M.S. Nasser [b], Matti Vuorinen [c]

[a] Aalto University, Department of Mathematics and System Analysis, P.O. Box 11100, FI–00076 Aalto, Finland
[b] Wichita State University, Department of Mathematics, Statistics, and Physics, Wichita, KS 67260-0033, USA
[c] University of Turku, Department of Mathematics and Statistics, FI–20014 University of Turku, Finland

ARTICLE INFO

MSC:
65E05
31A15
30C85

Keywords:
Conformal capacity
Condenser
Hyperbolic geometry
Boundary integral equation method
hp-FEM
Dirichlet problem

ABSTRACT

We consider constellations of disks which are unions of disjoint hyperbolic disks in the unit disk with fixed radii and unfixed centers. We study the problem of maximizing the conformal capacity of a constellation with a fixed number of disks under constraints on the centers in two cases. In the first case the constraint is that the centers are at most at distance $R \in (0, 1)$ from the origin and in the second case it is required that the centers are on the subsegment $[-R, R]$ of a diameter of the unit disk. We study also similar types of constellations with hyperbolic segments instead of the hyperbolic disks. Our computational experiments suggest that a dispersion phenomenon occurs: the disks/segments go as close to the unit circle as possible under these constraints and stay as far as possible from each other. The computation of capacity reduces to the Dirichlet problem for the Laplace equation which we solve using two methods: a fast boundary integral equation method and a high-order finite element method.

1. Introduction

In physics and chemistry there exist vast number of problems that involve interactions between multiple bodies or particles, such as the n-body problem of celestial mechanics and the many-body problem in quantum physics. Such interactions can be pairwise, such as forces, or complicated effects through some aggregate fields. Typically one is interested in configurations that imply some extremal state, for instance, minimum or maximum energy ones. These extremal configurations often have geometric features, such as symmetries, and give rise to many packing problems. One example of such problems is the modeling of intermolecular forces in simple systems using Lennard-Jones potential, which incorporates both short-range repulsion and long-range attraction [10,37]. The transition between repulsive and attractive forces occurs at a specific equilibrium distance defining the most stable configuration where the atoms forming the molecule prefer to remain.

Here we study condensers of the form $(\mathbb{B}^2, E)$ where for a fixed integer $m \geq 2$, the set E is a union of finitely many disjoint closed disks $E_1, \ldots, E_m$ in the unit disk $\mathbb{B}^2$ with fixed hyperbolic radii. We call such a collection of sets, or for that matter also the set E, *a constellation* of disks. Note that these disks are allowed to move: only the hyperbolic radii are fixed, but the centers are not. The location of the disks within a constellation has a strong influence on the numerical value of the conformal capacity. Our goal is to study extremal problems for the conformal capacity of condensers of the form $(\mathbb{B}^2, E)$ where $\mathbb{B}^2$ is the unit disk and the set $E \subset \mathbb{B}^2$ is a constellation of hyperbolic disks.

* Corresponding author.
E-mail addresses: Harri.Hakula@aalto.fi (H. Hakula), mms.nasser@wichita.edu (M.M.S. Nasser), vuorinen@utu.fi (M. Vuorinen).
[1] This work was supported by the Research Council of Finland (Flagship of Advanced Mathematics for Sensing Imaging and Modelling grant 359181).

https://doi.org/10.1016/j.camwa.2025.05.021
Received 26 April 2024; Received in revised form 24 March 2025; Accepted 24 May 2025

Available online 11 June 2025

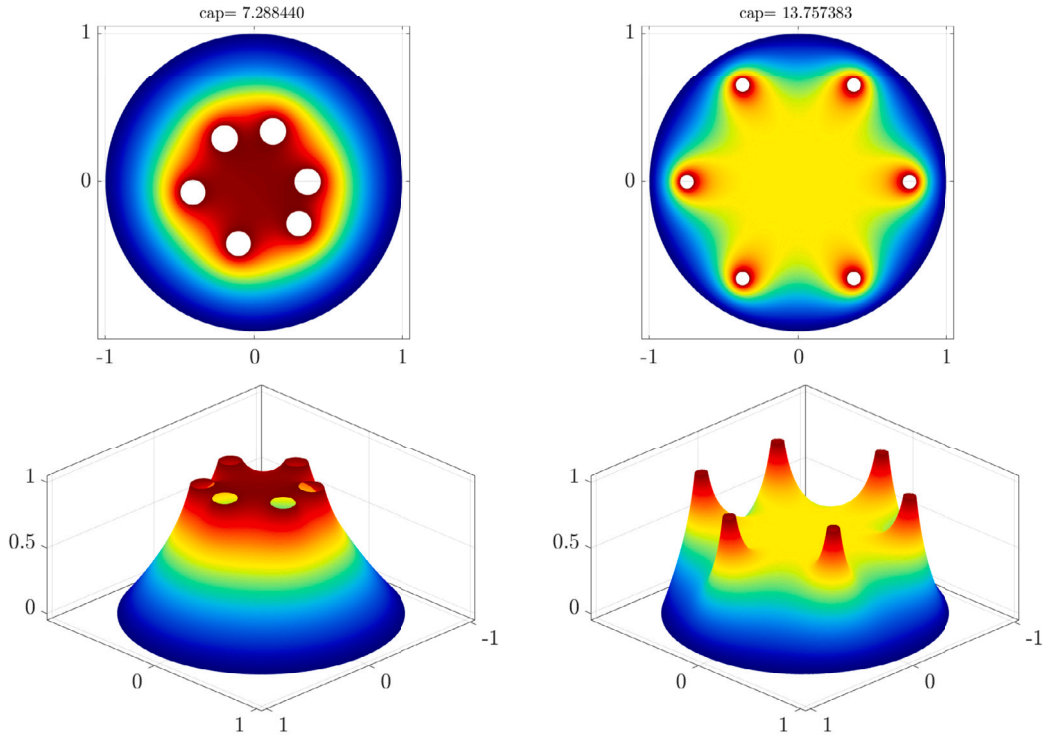

Fig. 1. Surface plots of the potentials for the six hyperbolic disks with equal hyperbolic radii 0.2. The centers of the disks are at the initial positions (left) and at the positions that maximize the capacity (right).

Classical results show that applying a geometric transformation, so called symmetrization, on a compact set $F \subset \mathbb{B}^2$, the new symmetrized set F^* exhibits some symmetry and what is relevant here, the new set F^* provides a lower bound for the conformal capacity [4,12,13,32]

$$\operatorname{cap}(\mathbb{B}^2, F) \geq \operatorname{cap}(\mathbb{B}^2, F^*). \tag{1.1}$$

Equality holds here if $F = F^*$. Due to the conformal invariance of the conformal capacity, in the case $F \neq F^*$, the lower bound (1.1) can be improved at least in the case when F is a constellation of separate hyperbolic disks. In the recent paper [16], the conformally invariant hyperbolic geometry was used as a key tool to refine (1.1).

We study here a reverse problem, maximization of conformal capacity. Symmetrization methods applied to a set E often reduce the distances between the points in E while some set functional like the area remains invariant. In the maximization process a reverse phenomenon can be naturally expected. Some results have been reported in literature [6,21]. Since the publication of the classical monograph [32], many authors have studied extremal problems from the point of view of potential theory [4,7,11,12,31,34].

It seems natural to study the problem of capacity maximization of a constellation under suitable constraints. We study two cases: (i) the centers of the disks of the constellation are contained in a subdisk, $E \subset B^2(0, R)$, (ii) the centers of the disks of the constellation are on a symmetric subsegment $[-R, R]$ on the diameter $(-1, 1)$ of $\mathbb{B}^2$. In both cases our simulations suggest that some kind of a maximal dispersion phenomenon occurs similar to what is observed for instance in chemistry: the disks increase their mutual "social distances" and, at the same time, have a tendency to move as close to the unit circle as the constraints permit. This phenomenon is the reason why a constraint for the centers of the disks is natural: without such a constraint, during the maximization process, the disks could go arbitrarily close to the unit circle and become "invisible", their Euclidean diameters would become arbitrarily small. Similar results are obtained when the hyperbolic disks in the above constellations are replaced by hyperbolic segments of fixed lengths such as radial hyperbolic segments and hyperbolic segments on the real line. Based on the numerical experiments we can predict the maximal capacities of all constellations exhibiting symmetry, that is, when the constellation in its extremal configuration can be divided into identical compartments of the unit disk.

1.1. Illustrative example

Consider a constellation E of six disks with equal hyperbolic radii whose centers are contained within a subdisk, $E \subset B^2(0, R)$. The task is to find a configuration with maximal capacity. This is illustrated in Fig. 1. Maximizing the capacity is equivalent to maximizing the L^2-norm of the gradient of the potential u which is a solution of the Dirichlet problem for the Laplace equation where the Dirichlet boundary values at the points of the unit circle are zero and at the boundary points of each disk equal to one. (For the formal definition of the capacity, see Section 2.3 below.)

Analyzing the results of optimization one can observe that, regardless of the initial configuration, two types of features of the final configuration of the constellation. First, the disks move towards the unit circle, as close as the constraint permits, and second, their mutual hyperbolic distances appear to become maximal, resulting in a symmetric configuration. This final configuration demonstrates what is referred to above as a maximal dispersion phenomenon.

1.2. Organization

The paper is organized as follows: Section 2 contains preliminary information about hyperbolic geometry, conformal capacity, and special functions to be used in the later sections. Section 3 is a description of our two computational methods, the *hp*-FEM and the boundary integral equation method. Our experimental discoveries are confirmed by these two methods. Section 4 presents our computational work on the disk constellations. Section 5 presents similar results, but now in place of the hyperbolic disks we have hyperbolic segments with fixed lengths. Section 6 draws the conclusions of our work and suggests problems for new research.

2. Preliminaries

In this section we recall some facts from hyperbolic geometry and special functions related to conformal capacity of canonical condensers.

2.1. Hyperbolic geometry

We recall some basic formulas and notation for hyperbolic geometry from [5]. The Euclidean balls with center $x \in \mathbb{R}^2$ and radius $r > 0$ are denoted $B^2(x, r)$ and its boundary sphere is $S(x, r)$. For brevity we write $\mathbb{B}^2 = B^2(0, 1)$. For $a, b \in \mathbb{B}^2$, the hyperbolic distance $\rho(a, b)$ between a and b is defined via the formula

$$\operatorname{sh}\frac{\rho(a,b)}{2} = \frac{|a-b|}{\sqrt{(1-|a|^2)(1-|b|^2)}}. \tag{2.1}$$

The hyperbolic disk with center $x \in \mathbb{B}^2$ and radius $R > 0$ is $B_\rho(x, R) = \{z : \rho(x, z) < R\}$. We often use the connection between the hyperbolic disk and Euclidean disk

$$\begin{cases} B_\rho(x,R) = B^2(y,r)\,, \\ y = \dfrac{x(1-t^2)}{1-|x|^2t^2}\,,\ r = \dfrac{(1-|x|^2)t}{1-|x|^2t^2}\,,\ t = \operatorname{th}(R/2)\,, \end{cases} \tag{2.2}$$

We use the notation sh and th for the hyperbolic sine and the hyperbolic tangent, respectively. Their inverse functions are arsh and arth.

2.2. Special functions

For $|z| < 1$, the Gaussian hypergeometric function is defined by the equality

$$ {}_2F_1(a,b;c;z) = \sum_{n=1}^{\infty} \frac{(a)_n (b)_n}{(c)_n} \frac{z^n}{n!},$$

where $(q)_n$ denotes the Pochhammer symbol, i.e. $(q)_n = q(q+1)\dots(q+(n-1))$ for every natural n and $(q)_0 = 1$ [1].

The complete elliptic integral of the first kind

$$\mathcal{K}(r) = \int_0^1 \frac{dt}{\sqrt{(1-t^2)(1-r^2t^2)}}, \quad r \in (0,1), \tag{2.3}$$

is, in fact, a special case of the Gaussian hypergeometric function; we have

$$\mathcal{K}(r) = \frac{\pi}{2}\, {}_2F_1(\tfrac{1}{2}, \tfrac{1}{2}; 1; r^2).$$

The decreasing homeomorphism $\mu : (0,1) \to (0,\infty)$

$$\mu(r) = \frac{\pi}{2}\frac{\mathcal{K}(\sqrt{1-r^2})}{\mathcal{K}(r)}, \quad 0 < r < 1,$$

is recurrent in the study of conformal invariants.

2.3. Condenser capacity

A *condenser* is a pair (G, E), where $G \subset \mathbb{B}^2$ is a domain and E is a compact non-empty subset of G. The *conformal capacity* of this condenser is defined as [12,14,19]

$$\operatorname{cap}(G, E) = \inf_{u \in A} \int_G |\nabla u|^2 \, dm, \tag{2.4}$$

where A is the class of $C_0^\infty(G)$ functions $u : G \to [0, \infty)$ with $u(x) \geq 1$ for all $x \in E$ and dm is the 2-dimensional Lebesgue measure. Here we assume that $G = \mathbb{B}^2$ is the unit disk and $E = \cup_{j=1}^m E_j$ where $E_1, \ldots, E_m$ are m compact disjoint non-empty subsets of the unit disk $\mathbb{B}^2$ such that $\partial E_1, \ldots, \partial E_m$ are smooth Jordan curves. Hence $\Omega = G \setminus E$ is a multiply connected domain of connectivity $m+1$ and the infimum in (2.4) is attained by a harmonic function u. This extremal function u is the unique solution of the Laplace equation in Ω with boundary values equal $u = 1$ on E and $u = 0$ on ∂G [12]. The capacity can be then expressed in terms of the extremal function u as

$$\operatorname{cap}(G, E) = \iint_\Omega |\nabla u|^2 \, dx \, dy, \tag{2.5}$$

which, using Green's formula [12, p. 4], implies that

$$\operatorname{cap}(G, E) = \int_{\partial \Omega} u \frac{\partial u}{\partial \mathbf{n}} \, ds \tag{2.6}$$

where $\partial u / \partial \mathbf{n}$ denotes the directional derivative of u along the outward normal. Since $u = 0$ on ∂G and $u = 1$ on ∂E_k, we have

$$\operatorname{cap}(G, E) = \sum_{k=1}^m b_k \tag{2.7}$$

where

$$b_k = \int_{\partial E_k} \frac{\partial u}{\partial \mathbf{n}} \, ds, \quad k = 1, 2, \ldots, m. \tag{2.8}$$

Thus, the constant b_k can be considered as the contribution of the compact set E_k to the capacity $\operatorname{cap}(G, E)$, for $k = 1, 2, \ldots, m$. Since the Dirichlet integral is conformally invariant, the cases for which $\partial E_1, \ldots, \partial E_m$ are rectilinear slits can be handled with the help of auxiliary conformal mappings which transform the slits to smooth curves.

The conformal capacity of a condenser is one of the key notions of potential theory of elliptic partial differential equations [14,20] and it has numerous applications to geometric function theory, both in the plane and in higher dimensions, [12,14,19,20].

Numerous variants of the definition (2.4) of capacity are given in [14,19]. For instance

$$\operatorname{cap}(G, E) = \mathsf{M}(\Delta(E, \partial G; G)), \tag{2.9}$$

where $\Delta(E, \partial G; G)$ is the family of all curves joining E with the boundary ∂G in the domain G and M stands for the modulus of a curve family [19, Ch 7]. A fundamental fact is *subadditivity*: if $E = \cup_{j=1}^m E_j$ where $E_j \subset \mathbb{B}^2$ for all j, then

$$\operatorname{cap}(\mathbb{B}^2, E) \leq \sum_{j=1}^m \operatorname{cap}(\mathbb{B}^2, E_j). \tag{2.10}$$

For the basic facts about capacities and moduli, the reader is referred to [12,14,19,20].

The exact value of the capacity is known only in a handful of special cases. For instance, the capacity $\gamma_2(r)$ of the Grötzsch condenser $(\mathbb{B}^2, [0, r])$ can be expressed as

$$\gamma_2(r) = 2\pi / \mu(r).$$

The capacity of an annulus is also known by the next lemma and (2.9).

Lemma 2.11. *[19, (7.3), p. 107]*
(1) If $0 < a < b$ *and* $D = \overline{B}^2(0, b) \setminus B^2(0, a)$,

$$\mathsf{M}(\Delta(S(0, a), S(0, b); D)) = 2\pi / \log(b/a).$$

(2) If $R > 0$ *then for* $x \in \mathbb{B}^2$

$$\mathsf{M}(\Delta(S(0, 1), B_\rho(x, R); \mathbb{B}^2)) = 2\pi / \log(1/\operatorname{th}(R/2)).$$

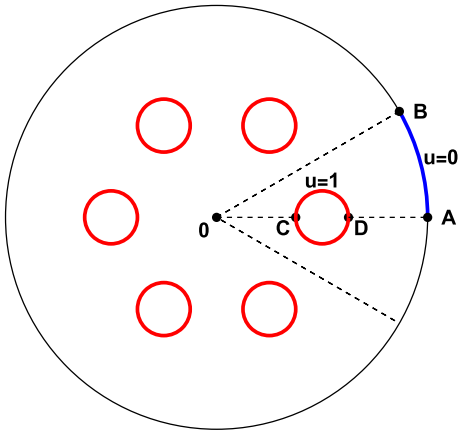

Fig. 2. Sectorial symmetry. The capacity of each sector or compartment can be computed separately. In the case of a constellation with identical elements, each compartment can be divided into two quadrilaterals symmetric with respect to the radius bisecting the sector.

2.4. Modulus of a quadrilateral

A *quadrilateral* is a Jordan domain Q on the complex plane with four marked points z_1, z_2, z_3, z_4 on the boundary. We assume that the points define positive orientation. By Riemann's mapping theorem, there is a conformal mapping of Q onto a rectangle with vertices $1, 1+hi, hi, 0$, $h>0$, such that the vertices of Q correspond to the vertices of the rectangle. Then the value h is called the conformal modulus of Q:

$$h = \mathrm{mod}Q \equiv \mathsf{M}(\Delta([0,1],[ih,1+ih];Q)).$$

An alternative method to find the modulus is to solve the following Dirichlet-Neumann boundary value problem for the Laplace equation [12]. Suppose that $\partial Q = \cup_{k=1}^4 \partial Q_k$; all the four boundary arcs between vertices are assumed to be non-degenerate. This problem is

$$\begin{cases} \Delta u &= 0, \quad \text{on} \quad Q, \\ u &= 1, \quad \text{on} \quad \partial Q_1 = (z_1, z_2), \\ u &= 0, \quad \text{on} \quad \partial Q_3 = (z_3, z_4), \\ \partial u/\partial n &= 0, \quad \text{on} \quad \partial Q_2 = (z_2, z_3), \\ \partial u/\partial n &= 0, \quad \text{on} \quad \partial Q_4 = (z_4, z_1). \end{cases}$$

In terms of a solution function u to the above problem, the modulus can be computed as

$$\iint_Q |\nabla u|^2 dm\,.$$

2.5. Symmetric compartments

If the constellation has suitable symmetry, like in the case of disks with equal size in Fig. 1, one can subdivide the domain into non-overlapping compartments, carry out the computation in each compartment. Due to symmetry, the result is equal for each compartment and we may thus reduce the computational load by a factor which in the case of m sets is roughly $1/(2m)$. To explain this idea further, we use moduli of quadrilaterals and refer to Fig. 2.

The disks $E_j, j=1,...,m$, of the constellation have equal radii and their centers are $r\exp(\mathrm{i}2k\pi/m), k=0,1,...,m, m=6$, for some $r\in(0,1)$ such that these m disks and the unit circle are not overlapping. The first compartment is $\{-\pi/m < \arg(z) < \pi/m\}$ and the first disk of the constellation is symmetric with respect to the real axis. In the upper half of the first compartment we consider the quadrilateral Q with vertices A, B, C, D and the associated Dirichlet-Neumann boundary value problem with $u(z)=1$ on the red semicircle and $u=0$ on the blue subarc of the unit circle and $\partial u/\partial n = 0$ on the dashed sides of the upper half of the compartment. Our conclusion is that

$$\mathrm{cap}(\mathbb{B}^2, E) = 2m\,\mathrm{mod}Q\,, \tag{2.12}$$

where $E = \cup_{j=1}^m E_j$. We can use this relation to predict the limiting value of the maximization of the capacity, e.g., of the constellation in Fig. 1. We present in Table 1 the numerical values of $\mathrm{cap}(\mathbb{B}^2, E)$ obtained using the BIE method and numerical values of $2m\,\mathrm{mod}Q$ obtained using the FEM for several values of m. We assume here that the disks $E_1, \dots, E_m$ are Euclidean disks such that the center and radius of the disk E_j is $0.5e^{\mathrm{i}2(j-1)\pi/m}$ and 0.1, $j=1,\dots,m$. The vertices of the quadrilateral in Fig. 2 are then $A=1$, $B=e^{\mathrm{i}\pi/m}$, $C=0.4$, and $D=0.6$.

Table 1
The numerical values of $\mathrm{cap}(\mathbb{B}^2, E)$ and $2m \bmod Q$.

m	$\mathrm{cap}(\mathbb{B}^2, E)$	$2m \bmod Q$	$\lvert\mathrm{cap}(\mathbb{B}^2, E) - 2m \bmod Q\rvert$
5	9.47487674904924	9.47487674904923	1×10^{-14}
6	10.0486182568334	10.04861825683339	1×10^{-14}
7	10.4636668610180	10.46366686101804	4×10^{-14}
8	10.7735173309461	10.77351733094614	4×10^{-14}

3. Methods

In this section the numerical methods used in the numerical experiments are briefly described. The capacities of constellations are computed using the boundary integral equation with the generalized Neumann kernel method (BIE) implemented in MATLAB and the *hp*-version of the finite element method (FEM) implemented in Mathematica. The maximization problems are computed using the interior-point method as implemented in MATLAB and Mathematica.

In any numerical study the questions of validation and verification need to be addressed. The Dirichlet problem (2.4) is one of the primary numerical model problems, therefore any standard solution technique can be viewed as having been validated. For example, for the constellations of disks case, i.e., when the domain Ω is a multiply connected circular domain of connectivity $m+1$, the Dirichlet problem (2.4) can be solved using linear combinations of m multi-valued analytic functions $v_1(z), \ldots, v_m(z)$ relevant to a special transcendental function known as the Schottky-Klein prime function associated with the circular domain Ω [8,9,24]. Two numerical methods have been presented in [9] for computing the m functions $v_1(z), \ldots, v_m(z)$. One of these methods is based on using the boundary integral equation with the generalized Neumann kernel that will be used in this paper. Computing these m functions $v_1(z), \ldots, v_m(z)$ requires solving m integral equations. Thus, in principle, the computational cost of computing these m functions using the integral equation and then using these m functions to compute the capacity is the same as the computational cost of using the integral equation to compute the capacity using the method discussed in this paper. Furthermore, explicit formulas for estimating the conformal capacity were derived in [24] by using the matching approach.

In the class of problems considered in this paper, verification follows through using two numerical methods. Namely, a high-order finite element method (*hp*-FEM) and a boundary integral equation method (BIE). This is illustrated with several numerical examples.

3.1. High-order finite element method

In contrast with the standard finite element method (*h*-version of FEM) the high-order finite element method adds a refinement parameter, the local polynomial order p, hence the name p-version. When both refinements are available we refer to *hp*-version. High-oder finite element methods have the capability for exponential convergence provided the discretization is constructed properly in both domain (in h) and local polynomial order (in p).

In this paper in all cases it is implicitly assumed that the exact parameterization of the boundaries on the parameter space is known. This allows us to benefit from efficient handling of large elements within the p-version without significant loss of accuracy, and more importantly, geometric refinements can be carried out with relative ease. This means that the number of elements can be kept relatively low.

Let us consider the Dirichlet problem (2.4) and its weak solution u_0. The following theorem due to Babuška and Guo [3], sets the limit to the rate of convergence of the *hp*-FEM. Notice that construction of the appropriate spaces is technical, but can be extended to parameterised surfaces. For rigorous treatment of the theory involved, see Schwab [33] and references therein.

Theorem 3.1. *Let the computational domain $G \subset \mathbb{R}^2$, v the FEM-solution of (2.4), and let the weak solution u_0 be in a suitable countably normed space where the derivatives of arbitrarily high order are controlled. Then*

$$\inf_v \|u_0 - v\|_{H^1(G)} \le C \exp(-b\sqrt[3]{N}),$$

where C and b are independent of N, the number of degrees of freedom. Here v is computed on a proper geometric mesh, where the order of an individual element is set to be its element graph distance to the nearest singularity. (The result also holds for meshes with constant polynomial degree.)

There are many efficient error estimators available for *hp*-FEM. The so-called auxiliary subspace error estimation fits particularly well within our implementation. Let $\mathcal{T}$ be some *hp*-discretization on the computational domain G. Assuming that the exact solution $u \in H_0^1(G)$, defined on $\mathcal{T}$, has finite energy, the approximation problem is as follows: Find $\hat{u} \in V$ such that

$$a(\hat{u}, v) = l(v) \ (= a(u, v)) \quad (\forall v \in V), \tag{3.2}$$

where $a(\cdot, \cdot)$ and $l(\cdot)$, are the bilinear form and the load potential, respectively. Additional degrees of freedom are introduced by enriching the space V via introduction of an auxiliary subspace or "error space" $W \subset H_0^1(G)$ such that $V \cap W = \{0\}$. The error problem becomes thus: Find $\varepsilon \in W$ such that

$$a(\varepsilon, v) = l(v) - a(\hat{u}, v) (= a(u - \hat{u}, v)) \quad (\forall v \in W). \tag{3.3}$$

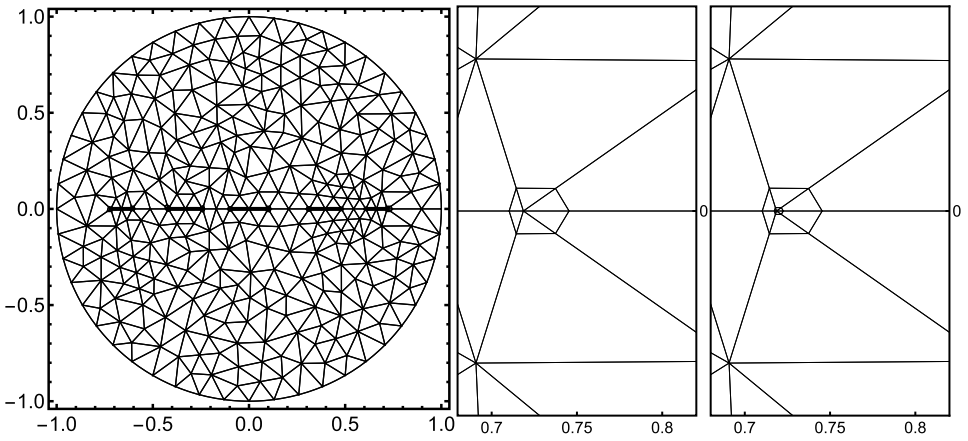

Fig. 3. Mesh refinements. Left: FEM mesh with the five segments on the diameter indicated with thick lines. Middle: A detail of the mesh at one of the end points of the segments after one application of the replacement rule. Right: Successive levels of refinements, eight altogether, are shown in the plot (the smallest ones are not visible in the given scale).

This can be interpreted as a projection of the residual to the auxiliary space.

The main result on this kind of estimators for the Dirichlet problem (2.4) is given in [17]. It should be mentioned that it is generally accepted that the constant K appearing in the theorem below is in fact independent of p, yet no rigorous proofs exist to support this observation.

Theorem 3.4 *([17]). There exist a constant K depending only on the dimension d and polynomial degree p, continuity and coercivity constants C and c, and the shape-regularity of the triangulation $\mathcal{T}$ such that*

$$\frac{c}{C}\,\|\varepsilon\|_1 \le \|u-\hat{u}\|_1 \le K(d,p)\left(\|\varepsilon\|_1 + \operatorname{osc}(R,r,\mathcal{T})\right),$$

where the residual oscillation depends on the volumetric and face residuals R and r, and the triangulation $\mathcal{T}$.

3.2. A priori refinement strategies

In the classes of geometries considered here, two implementation challenges have to be met to obtain the optimal exponential convergence. First, for the slits, we must have geometric refinements of the elements at the singularities. Second, for circular boundaries, the element boundaries must retain the exact parameterization.

In problems with singularities with known locations, a priori optimally refined meshes can be computed using rule based algorithms [18]. The geometric refinement process is illustrated in Fig. 3: First a geometrically conforming mesh is generated such that every singularity is isolated, that is, local refinement rules can be applied simultaneously without violating the conformity of the mesh. Each local refinement can be applied multiple times in a nested fashion. One of the drawbacks of this approach is that unwinding local refinements is difficult, since typical geometric invariants of the triangulations are not valid within the local refinements, for instance, the Delaunay property (maximization of the minimal angle). In the solution process we are content to adapt the discretization simply by modifying the a priori strategy, in other words, by remeshing the whole domain.

For problems with circular boundaries, each element at the boundary is curved with geometrically faithful parameterization. One example with associated detail is shown in Fig. 4.

3.3. BIE method

We shall consider two types of condensers $(\mathbb{B}^2, E)$ in this paper. In the first type, the compact set E is assumed to be the union of m disjoint hyperbolic disks in $\mathbb{B}^2$. For the second type, we assumed that E is the union of m disjoint hyperbolic segments in $\mathbb{B}^2$. For both types of domains, the capacity $\operatorname{cap}(\mathbb{B}^2, E)$ can be computed using the boundary integral equation (BIE) method presented in [28]. The method is based on the BIE with the generalized Neumann kernel. This method is briefly reviewed in this section. However, before implementing the numerical method, we first convert the hyperbolic disks and segments to Euclidean ones, using (2.2).

3.3.1. Domains bounded by smooth curves

When E is a union of m disjoint hyperbolic disks, then the domain $\Omega = \mathbb{B}^2 \setminus E$ is a bounded multiply connected domain of connectivity $m+1$ whose boundaries are circles. The orientation of the external circle C_0 is counterclockwise oriented and the inner circles $C_1, \ldots, C_m$ are clockwise oriented. The external circle C_0 is parametrized by $\eta_0(t)$ for $t \in J_0 = [0, 2\pi]$. Each inner circle C_j is parametrized by $\eta_j(t)$, $t \in J_j = [0, 2\pi]$, for $j = 1, 2, \ldots, m$. Let J be the disjoint union of the $m+1$ intervals $J_j = [0, 2\pi]$, $j = 0, 1, \ldots, m$. We define a parameterization of the whole boundary $C = \cup_{j=0}^{m} C_j$ on J by (see [26] for the details)

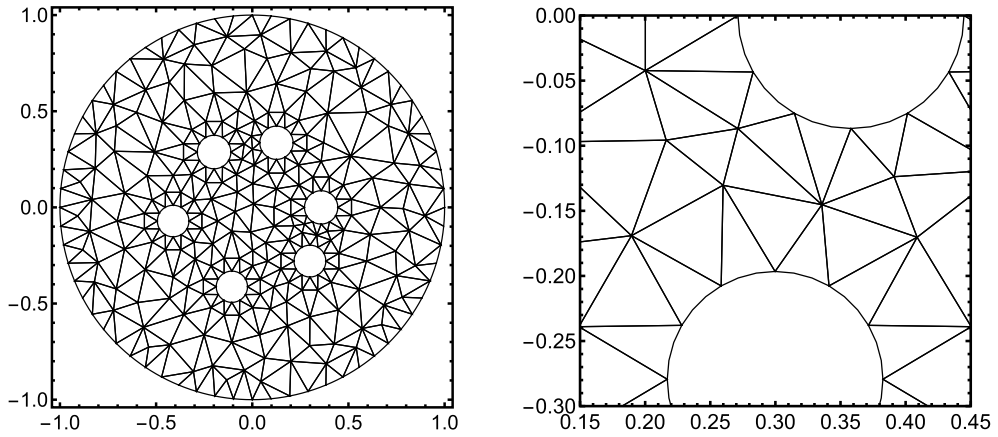

Fig. 4. Curved elements. Left: FEM mesh with six disks. Right: A detail showing the curved edges.

$$\eta(t) = \begin{cases} \eta_0(t), & t \in J_0, \\ \eta_1(t), & t \in J_1, \\ \vdots & \\ \eta_m(t), & t \in J_m. \end{cases}$$

With the parameterization $\eta(t)$ of the whole boundary C, we define a complex function A by

$$A(t) = \eta(t) - \alpha, \tag{3.5}$$

where α is a given point in the domain Ω. For each $k = 1, 2, \ldots, m$, let z_k be a given point interior to the circle C_k, let the function γ_k be defined by

$$\gamma_k(t) = \log|\eta(t) - z_k|, \tag{3.6}$$

and let μ_k be the unique solution of the BIE

$$\mu_k - \mathbf{N}\mu_k = -\mathbf{M}\gamma_k, \tag{3.7}$$

where $\mathbf{N}$ is the integral operator with the generalized Neumann kernel

$$N(s,t) := \frac{1}{\pi} \operatorname{Im}\left(\frac{A(s)}{A(t)} \frac{\eta'(t)}{\eta(t) - \eta(s)} \right), \quad (s,t) \in J \times J, \tag{3.8}$$

and $\mathbf{M}$ is the integral operator with the kernel

$$M(s,t) := \frac{1}{\pi} \operatorname{Re}\left(\frac{A(s)}{A(t)} \frac{\eta'(t)}{\eta(t) - \eta(s)} \right), \quad (s,t) \in J \times J. \tag{3.9}$$

Then the function h_k given by

$$h_k = [\mathbf{M}\mu_k - (\mathbf{I} - \mathbf{N})\gamma_k]/2 \tag{3.10}$$

is a piecewise constant function, i.e.,

$$h_k(t) = \begin{cases} h_{0,k}, & t \in J_0, \\ h_{1,k}, & t \in J_1, \\ \vdots & \\ h_{m,k}, & t \in J_m, \end{cases}$$

where $h_{0,k}, h_{1,k}, \ldots, h_{m,k}$, $k = 1, 2, \ldots, m$, are real constants. The capacity $\operatorname{cap}(\mathbb{B}^2, E)$ can be then computed by [28, Eq. (3.9)]

$$\operatorname{cap}(\mathbb{B}^2, E) = 2\pi \sum_{k=1}^{m} a_k, \tag{3.11}$$

where the values of the m real constants $a_1, \ldots, a_m$ are computed by solving the $(m+1) \times (m+1)$ linear system

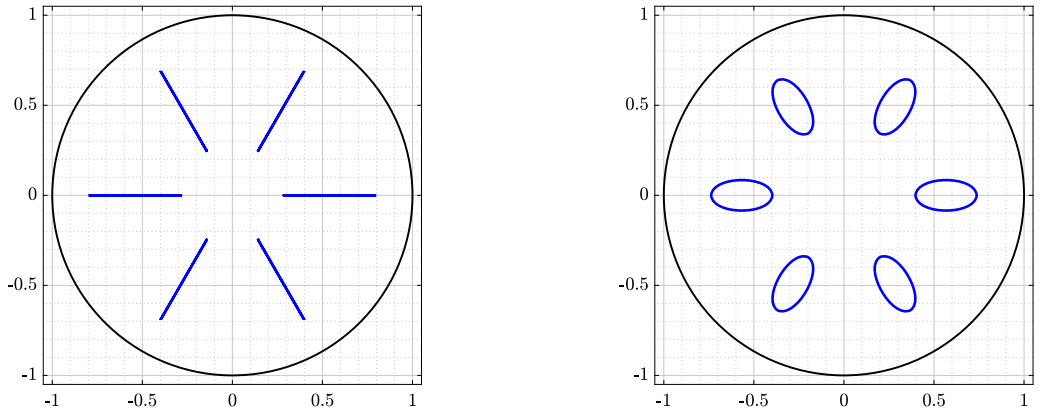

Fig. 5. A schematic of a given bounded multiply connected domain Ω interior to the unit circle and exterior to m radial slits (left) and its conformally equivalent computed domain D interior to the unit circle and exterior to m smooth Jordan curves (right) for $m = 6$.

$$\begin{bmatrix} h_{0,1} & h_{0,2} & \cdots & h_{0,m} & 1 \\ h_{1,1} & h_{1,2} & \cdots & h_{1,m} & 1 \\ \vdots & \vdots & \ddots & \vdots & \vdots \\ h_{m,1} & h_{m,2} & \cdots & h_{m,m} & 1 \end{bmatrix} \begin{bmatrix} a_1 \\ a_2 \\ \vdots \\ a_m \\ c \end{bmatrix} = \begin{bmatrix} 0 \\ 1 \\ \vdots \\ 1 \end{bmatrix}. \tag{3.12}$$

The constants $b_1, \ldots, b_m$ in (2.8) are related to the constants $a_1, \ldots, a_m$ by

$$b_k = 2\pi a_k, \quad k = 1, 2, \ldots, m. \tag{3.13}$$

The BIE (3.7) can be discretized by the Nyström method with the trapezoidal rule to obtain an $(m+1)n \times (m+1)n$ linear system where n is the number of the discretization points in each boundary component. The linear system can then be solved by the MATLAB function `gmres` and the matrix-vector product in `gmres` can be computed in $O(mn)$ operations using the MATLAB function `zfmm2dpart` from the fast multipole method (FMM) MATLAB toolbox FMMLIB2D [15]. The boundary components of the domain Ω are circles and hence the integrands in (3.7) and (3.10) are analytic. Thus the trapezoidal rule converges exponentially with $O(e^{-\sigma n})$ when it is used to discretize the integrals in (3.7) and (3.10) [36]. The constant σ depends on the configuration of the domain Ω as well as the auxiliary point α. The numerical solution of the integral equation will then converge with a similar rate of convergence as the trapezoidal rule [2]. This method for solving the BIE (3.7) was implemented in the MATLAB function `fbie` presented in [26]. The MATLAB function `fbie` provides us with approximations to the solution μ_k of the BIE (3.7) as well as the piecewise constant function h_k in (3.10). The computed values of h_k are used to set up the $(m+1) \times (m+1)$ linear system (3.12), which will be solved using the Gauss elimination method (here $m+1$ is the number of boundary components of the domain G which is usually small). By computing the constants $a_1, \ldots, a_m$, the value of the capacity $\operatorname{cap}(G, E)$ is given by (3.11). Further, the values of the constants $b_1, \ldots, b_m$ are given by (3.13). See [26,28] for details.

3.3.2. *Domains bounded by slits*

The BIE method presented above can be used to compute the capacity of only condensers bounded by smooth or piecewise Jordan curves [26,28]. Since the Dirichlet integral is conformally invariant, the capacities for the cases for which the plates of the condenser are slits can be computed with the help of conformal mappings. In this paper, we consider two types of domains Ω bounded by slits.

In the first case, we assume that Ω is the unit disk with m radial slits. For such a case, we can use the iterative method presented in [27] to compute a conformally equivalent domain D bounded by smooth Jordan curves so that our method presented in Section 3.3.1 can be used. A schematic of the domain Ω and its conformally equivalent computed domain D for $m = 6$ is presented in Fig. 5.

In the second case, we assume that Ω is the unit disk with m rectilinear slits on the real line (see Fig. 6 (left) for $m = 5$). Unlike the domain in the first case, this domain is not one of the canonical slit domains (see [22,25]). Thus, in this case, we first consider the unbounded domain $\hat{\Omega}$ in the exterior of the m rectilinear slits which is a canonical slit domain (see Fig. 7 (left) for $m = 5$). We use the iterative method presented in [27] to compute a conformally equivalent domain $\hat{D}$ in the exterior of m smooth Jordan curves and the conformal mapping $w = \Phi(z)$ from the domain $\hat{D}$ onto $\hat{\Omega}$ (see Fig. 7 (right) for $m = 5$). Hence, $z = \Phi^{-1}(w)$ is a conformal mapping from the domain $\hat{\Omega}$ onto $\hat{D}$. Since the unit circle is in the interior of the domain $\hat{\Omega}$, the conformal mapping $z = \Phi^{-1}(w)$ can be used to compute the image of the unit circle which will be a smooth Jordan curve exterior to the computed m smooth Jordan curves. Thus, the conformal mapping $z = \Phi^{-1}(w)$ maps the given domain Ω onto a conformally equivalent domain D bounded by smooth Jordan curves so that the method reviewed in Section 3.3.1 can be used (see Fig. 6 (right) for $m = 5$). Notice that the external curve in Fig. 6 (right) is not a circle.

For details on the iterative method for computing the domain D for both cases of slit domains discussed above, we refer the reader to [27] (see also [21] for other types of slit domains).

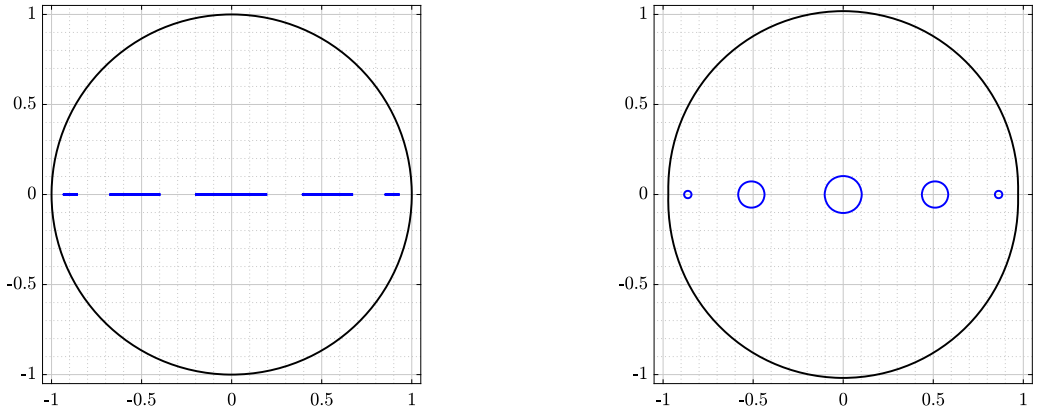

Fig. 6. A schematic of a given bounded multiply connected domain Ω interior to the unit circle and exterior to m rectilinear slits (left) and its conformally equivalent computed domain D bounded by $m+1$ smooth Jordan curves (right) for $m=5$.

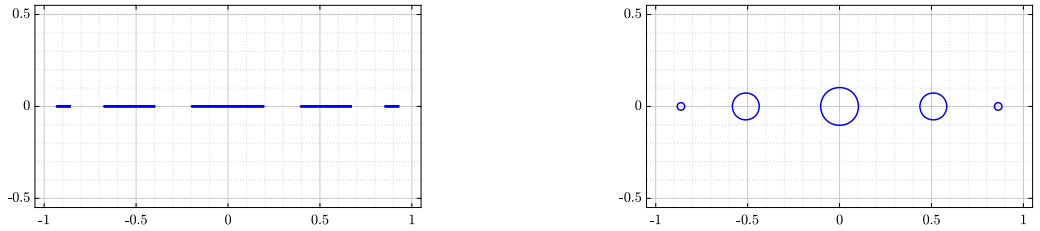

Fig. 7. A schematic of a given unbounded multiply connected domain $\hat{\Omega}$ exterior to m rectilinear slits (left) and its conformally equivalent computed domain $\hat{D}$ exterior to m smooth Jordan curves (right) for $m=5$.

3.4. Nonlinear optimization: interior-point method

The numerical optimization algorithm of our choice is the interior-point method as implemented in Mathematica (`FindMaximum`, [38]) and Matlab (`fmaxcon`, [23]). The task is to find an optimal configuration for a constellation of hyperbolic disks E with fixed radii, where at every step the current configuration is solved using either one of the methods described above. The standard textbook reference is Nocedal and Wright [30].

In the most general case the problem is defined as in (3.14), where the only constraints are geometric ones, that is, the disks are not allowed to overlap, and they are not allowed to drift to the boundary, for instance, they must lie within a disk $B^2(0,R)$ with same prescribed radius R, or alternatively their centers must lie inside some constraining disk. The radii are fixed and the optimization concerns only the locations of the disks. For example, for the constellation of six hyperbolic disks with the initial positions shown in Fig. 1 (left), the positions of the centers of the six disks during the optimization process are shown in Fig. 8 where the red dots correspond to the initial positions (Fig. 1 (left)) and the maximal positions (Fig. 1 (right)).

The maximization problem is formally defined as

$$\begin{aligned} \max_{E} \quad & \operatorname{cap}(\mathbb{B}^2, E) \\ \text{subject to:} \quad & E_i \cap E_j = \emptyset \qquad \forall\, i,j = 1,\dots,m, i \neq j \\ & E_j \subset B^2(0,R) \quad \forall\, j = 1,\dots,m. \end{aligned} \tag{3.14}$$

This nonlinear optimization problem can be solved using the interior-point method, and the solution would be a local maximum.

Notice, that the objective function is indeed the capacity of the constellation. The number of evaluations needed for the optimization is greater than the number of iteration steps, since the gradients and Hessians must be approximated numerically. One of the insights gained over many such computations is that the optimization depends on the high accuracy of the capacity solver, since otherwise the approximate derivatives are not sufficiently accurate.

In the context of this work, there have been no attempts to devise a special method that would incorporate some of the insights gathered during this study. Instead, the numerical optimization is used to challenge those insights and therefore the optimizations have been computed with minimal input information.

4. Numerical experiments: constellations of circular domains

In this section the focus is on constellations of disks. In the maximization of the capacity the positions of the disks are subject to two types of geometric constraints, they are either constrained to a disk of given radius or an interval of fixed length on the real

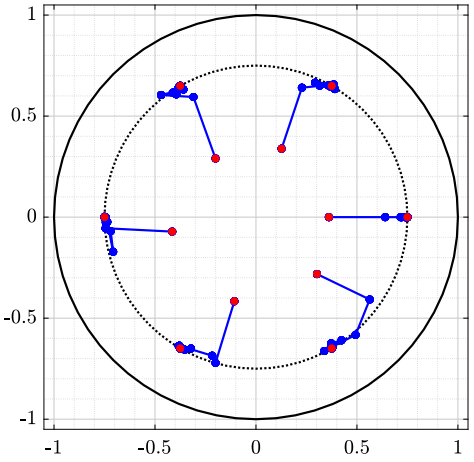

Fig. 8. The positions of the centers of the six disks in Fig. 1 during the optimization process using the BIE method. The red dots corresponding to the initial positions (Fig. 1 (left)) and the maximal positions (Fig. 1 (right)).

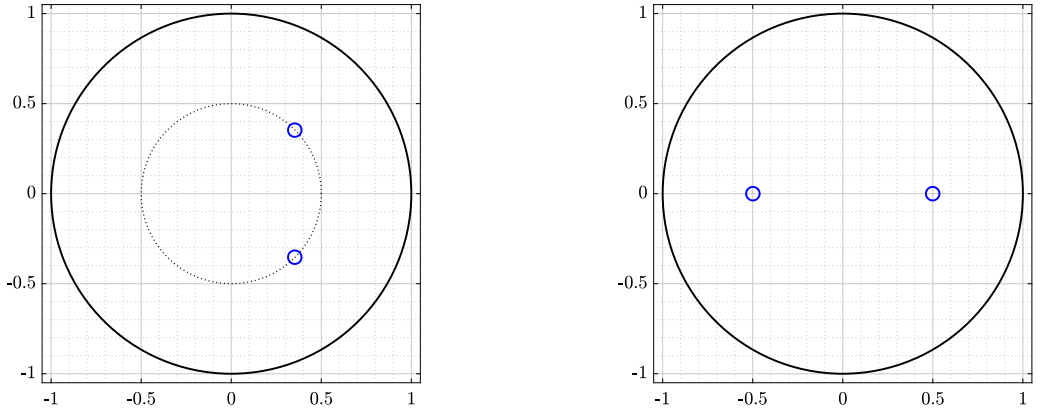

Fig. 9. Two hyperbolic disks with hyperbolic radius 0.1. The centers of the two disks are $Re^{\pm i\theta}$ for $R = 0.5$ and $\theta = \pi/4$ (left) and $\pm x$ for $x = 0.5$ (right).

line. The experiments in turn either cover full parameter ranges or are general in the sense that the initial configurations are random, but satisfy the constraints, of course. We first consider constellations of two disks of equal hyperbolic radii, and then extend the investigation to constellations with six disks constrained to a disk, and to constellations with five disks with centers constrained to an interval. In the two latter cases also the case of unequal hyperbolic radii is studied. In the final experiment the constellation is condensed into a single disk with equal capacity. The objective is to compare the hyperbolic area and perimeter of a constellation to that of a condensed one.

4.1. Constellation of two disks with constrained positions

We begin with the constellation E, union of two hyperbolic disks D_1 and D_2 with equal hyperbolic radius r. First we assume that the centers of these disks are on $Re^{\pm i\theta}$ where $0 < \theta_{\min} < \theta < \pi - \theta_{\min} < \pi$ and

$$\theta_{\min} = \arcsin\left(\frac{(1-R^2)\operatorname{sh} r}{2R}\right).$$

See Fig. 9 (left) for $R = 0.5$ and $\theta = \pi/4$. The two disks touch each other when $\theta = \theta_{\min}$ or $\theta = \pi - \theta_{\min}$. When $r = 0.1$, the values of $\operatorname{cap}(\mathbb{B}^2, E)$ vs. θ are shown in Fig. 10 (left) for several values of R.

Then we assume that the centers of these disks are on $\pm x$ where $x_{\min} < x < 1$ and $x_{\min} = \operatorname{th}(r/2)$ where the two disks touch each other when $x = x_{\min}$ (See Fig. 9 (right) for $x = 0.5$). The values of $\operatorname{cap}(\mathbb{B}^2, E)$ for $r = 0.1$ vs. x are shown in Fig. 10 (right).

Note that $\operatorname{cap}(\mathbb{B}^2, D_i) = -2\pi/\log(\operatorname{th}(r/2))$, $i = 1, 2$. For $r = 0.1$, the values of $\operatorname{cap}(\mathbb{B}^2, D_1)$ are shown in Fig. 10 as "dashed line" and the values of $\operatorname{cap}(\mathbb{B}^2, D_1) + \operatorname{cap}(\mathbb{B}^2, D_2)$ as "dotted line."

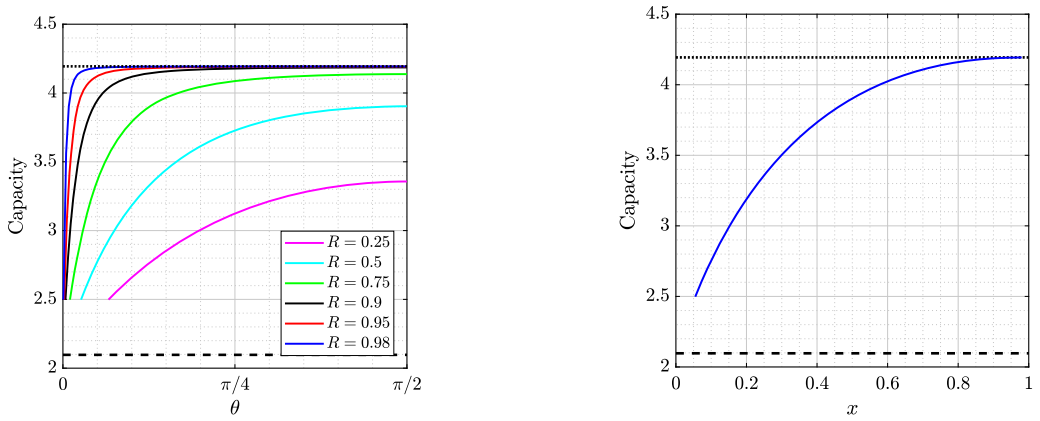

Fig. 10. The capacity for two hyperbolic disks with hyperbolic radius $r = 0.1$. The centers of the two disks are $Re^{\pm i\theta}$ (left) and $\pm x$ (right), where the leftmost point on the curve corresponds to Cartesian coordinate $\text{th}(r/2) \approx 0.05$, that is, when the two disks touch.

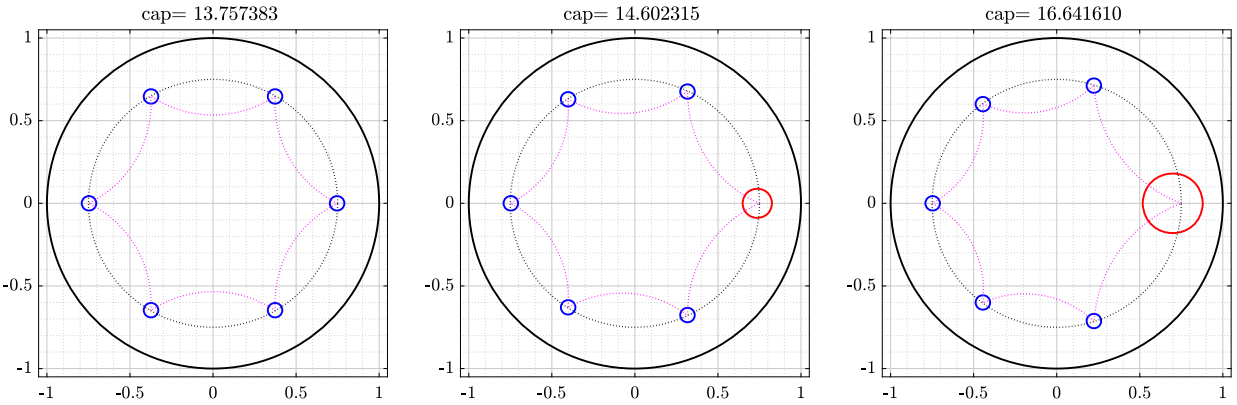

Fig. 11. Disk 1 has hyperbolic radius 0.2 (left), 0.4 (center), and 0.8 (right). Disks 2 through 6 have hyperbolic radii 0.2.

Table 2
The hyperbolic distances between the centers of consecutive disks in Fig. 11.

Case	Capacity	$\rho(z_1, z_2)$	$\rho(z_2, z_3)$	$\rho(z_3, z_4)$	$\rho(z_4, z_5)$	$\rho(z_5, z_6)$	$\rho(z_6, z_1)$
A	13.7574	2.6161	2.6161	2.6161	2.6161	2.6161	2.6161
B	14.6023	2.7393	2.5532	2.5482	2.5482	2.5532	2.7393
C	16.6416	2.9128	2.4504	2.4363	2.4363	2.4504	2.9128

4.2. Constellation of six disks constrained to a disk

We increase the number of disks and consider the positions of a constellation of six hyperbolic disks that maximize the capacity $\text{cap}(\mathbb{B}^2, E)$ under the constraint that the hyperbolic centers of these disks are inside the Euclidean disk $|z| \le R$ (we assume in the examples below that $R = 0.75$). The disks are numbered D_1 to D_6 in counterclockwise orientation. We denote the center of the disk D_j by z_j, $j = 1, \ldots, 6$. Without any loss of generality, we assume that the center z_1 of the disk D_1 lies on the positive real axis.

First we assume that all six disks have equal hyperbolic radii = 0.2, and the initial positions are random within the given constraints. The configuration which maximizes the capacity $\text{cap}(\mathbb{B}^2, E)$ has the maximal dispersion property: The positions of these six disks are on the Euclidean circle $|z| = R$ and, moreover, are symmetric, that is, the hyperbolic distances between the centers of any two adjacent disks are equal (see Fig. 11 (left) and Table 2). The computed capacity = 13.757381.

When the hyperbolic radius of one of these disks is changed either to 0.4 (see Fig. 11 (center)) or 0.8 (see Fig. 11 (right)), the centers of the other disks move away from the larger disk (see Table 2), yet rotational symmetry is preserved for the maximal configuration. To study closely the impact of increasing the hyperbolic radius of only one disk on the positions that maximize the capacity $\text{cap}(\mathbb{B}^2, E)$, we assume that the hyperbolic radius of the first disk D_1 is r_1 and the hyperbolic radii of the remaining five disks D_2–D_6 are 0.2. As above, we find the positions of these six disks that maximize the capacity $\text{cap}(\mathbb{B}^2, E)$ under the above constraint. For the positions that maximizes the capacity $\text{cap}(\mathbb{B}^2, E)$, we compute the hyperbolic distances $\rho(z_1, z_2)$, $\rho(z_2, z_3)$, and $\rho(z_3, z_4)$ and the values of the constants b_1, b_2, b_3, and b_4 in (3.13) where the values of r_1 are changing from 0.2 to 2. The obtained numerical

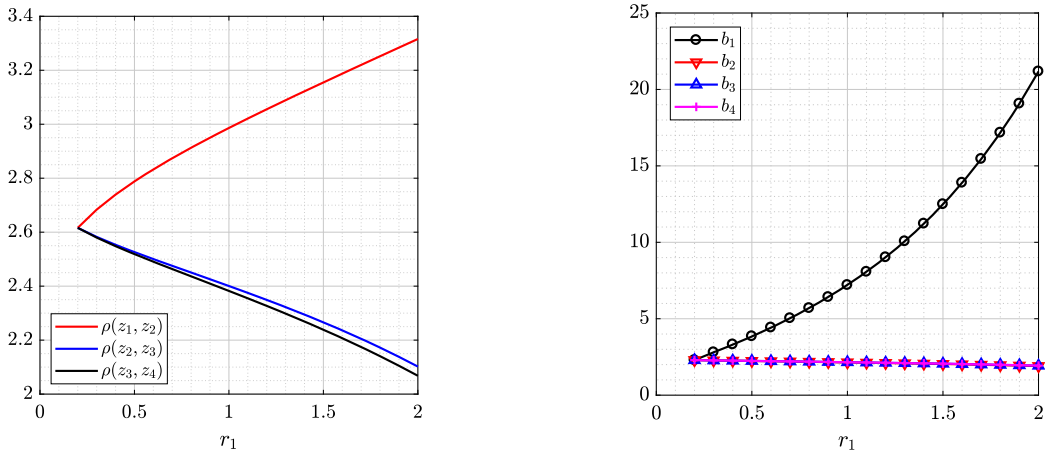

Fig. 12. The hyperbolic distances between the centers of consecutive disks (left) and the values of the constants b_1, b_2, b_3, and b_4 in (2.8) (right) as functions of r_1.

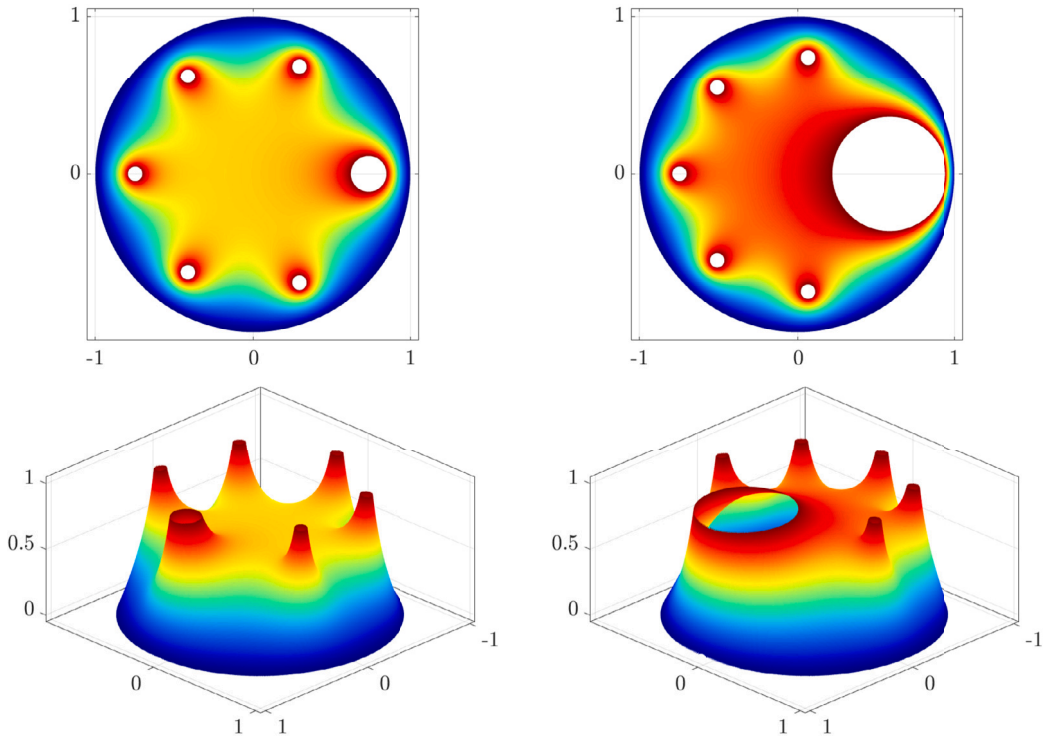

Fig. 13. Surface plots of the potentials for the six hyperbolic disks where the Disk 1 has hyperbolic radius r_1 and Disks 2 through 6 have hyperbolic radii 0.2 for $r_1 = 0.5$ (left) and $r_1 = 1.5$ (right). The centers are at the positions that maximize the capacity.

results are presented in Fig. 12. Notice that the constant b_k can be regarded as the contribution of the disk set D_k to the capacity $\mathrm{cap}(G, E)$, for $k = 1, 2, \ldots, m$. As we can see, the values of b_1 increased as r_1 increased and the values of b_2, b_3, and b_4 are almost constants. Notice also that, due to symmetry, $\rho(z_1, z_2) = \rho(z_1, z_6)$, $\rho(z_2, z_3) = \rho(z_6, z_5)$, $\rho(z_3, z_4) = \rho(z_5, z_4)$, $b_5 = b_3$, and $b_6 = b_2$. See Fig. 13.

If the hyperbolic radii of two of these six disks are changed to either 0.4 or 0.8, the natural symmetries induce three local maxima as shown in Fig. 14. The hyperbolic distances between the centers of any two adjacent disks for all cases in Fig. 14 are shown in Table 3. Similarly, with three disks three local maxima are observed (see Fig. 15 and Table 4).

Considering the results for constellations of disks with unequal radii we can observe that in all cases the maximal dispersion property is again observed: In the configuration which maximizes the capacity $\mathrm{cap}(\mathbb{B}^2, E)$ the positions of these six disks are on the Euclidean circle $|z| = R$.

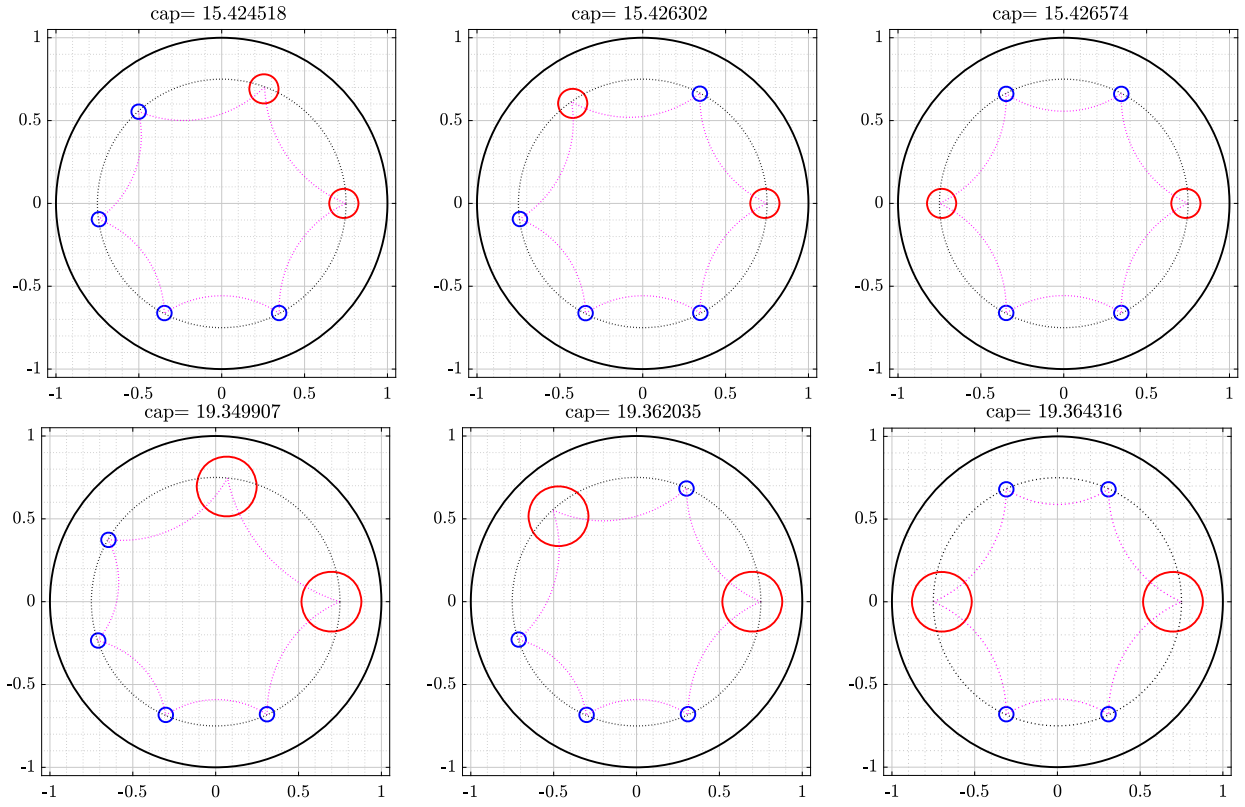

Fig. 14. First row: Four disks with hyperbolic radii 0.2 and two disks with hyperbolic radii 0.4. Second row: Four disks with hyperbolic radii 0.2 and two disks with hyperbolic radii 0.8.

Table 3
The hyperbolic distances between the centers of consecutive disks in Fig. 14.

Case	Capacity	$\rho(z_1,z_2)$	$\rho(z_2,z_3)$	$\rho(z_3,z_4)$	$\rho(z_4,z_5)$	$\rho(z_5,z_6)$	$\rho(z_6,z_1)$
A	15.4245	2.8523	2.6767	2.4861	2.4815	2.4861	2.6767
B	15.4263	2.6800	2.6800	2.6742	2.4867	2.4867	2.6742
C	15.4266	2.6747	2.4920	2.6747	2.6747	2.4920	2.6747
D	19.3499	3.1452	2.7534	2.2784	2.2672	2.2784	2.7534
E	19.3620	2.7700	2.7700	2.7519	2.2813	2.2813	2.7519
F	19.3643	2.7553	2.2965	2.7553	2.7553	2.2965	2.7553

Table 4
The hyperbolic distances between the centers of consecutive disks in Fig. 15.

Case	Capacity	$\rho(z_1,z_2)$	$\rho(z_2,z_3)$	$\rho(z_3,z_4)$	$\rho(z_4,z_5)$	$\rho(z_5,z_6)$	$\rho(z_6,z_1)$
A	16.2261	2.7931	2.7931	2.6126	2.4210	2.4210	2.6126
B	16.2280	2.7903	2.6189	2.6161	2.6108	2.4263	2.6135
C	16.2295	2.6161	2.6161	2.6161	2.6161	2.6161	2.6161
D	21.9116	3.0047	3.0047	2.6025	2.1205	2.1205	2.6025
E	21.9225	3.0015	2.6190	2.6172	2.6035	2.1336	2.6053
F	21.9307	2.6161	2.6161	2.6161	2.6161	2.6161	2.6161

4.3. Constellation of five disks constrained to the real line

Next we consider a constellation of five hyperbolic disks under the constraint that the hyperbolic centers of these disks lie within the interval $[-R, R]$. The disks are numbered $(D_1, \ldots, D_5)$ from left to right, and $R = 0.75$ in all experiments.

The set of experiments follows that of the previous section. Four cases are considered: (a) all five disks have equal hyperbolic radii $= 0.2$, (b) one of the disks has radius $= 0.4$, (c) two disks have radius $= 0.4$, and finally (d) three disks have radius $= 0.4$.

All configurations up to symmetry are summarized in Figs. 16, 17, 18, and Tables 5, 6, 7, for (a) and (b), (c), and (d), respectively. The maximal configurations exhibit the maximal dispersion property on a diameter: D_1 and D_5 lie at the end points of the interval,

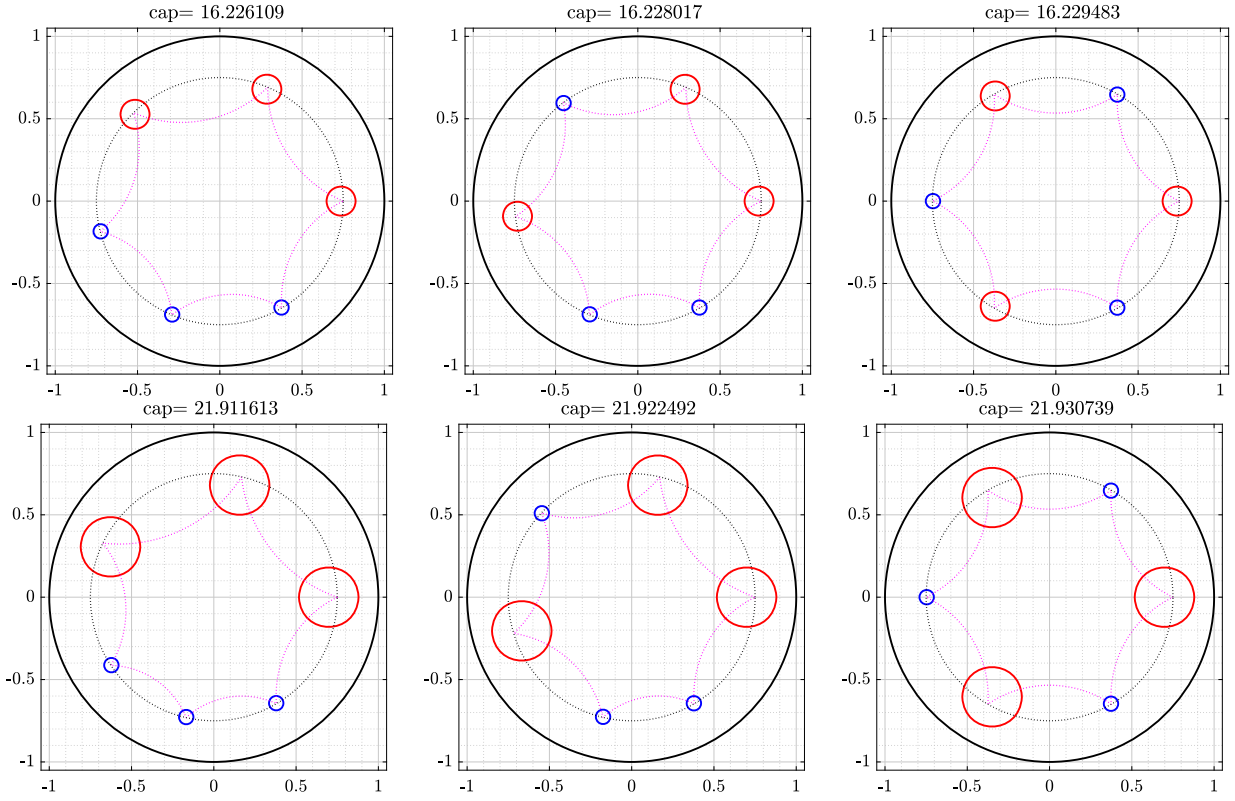

Fig. 15. First row: Three disks with hyperbolic radii 0.2 and three disks with hyperbolic radii 0.4. Second row: Three disks with hyperbolic radii 0.2 and three disks with hyperbolic radii 0.8.

Table 5
The hyperbolic distances between the centers of consecutive disks in Fig. 16.

Case	Capacity	$\rho(z_1, z_2)$	$\rho(z_2, z_3)$	$\rho(z_3, z_4)$	$\rho(z_4, z_5)$
A	8.0200	0.9467	0.9992	0.99920	0.9467
B	8.7506	1.2166	0.9160	0.90604	0.8532
C	8.3928	1.0656	1.1689	0.85703	0.8003
D	8.3855	0.7943	1.1516	1.1516	0.7943

Table 6
The hyperbolic distances between the centers of consecutive disks in Fig. 17.

Case	Capacity	$\rho(z_1, z_2)$	$\rho(z_2, z_3)$	$\rho(z_3, z_4)$	$\rho(z_4, z_5)$
A	9.0727	1.3935	1.0596	0.7477	0.6910
B	9.0793	1.0701	1.0777	1.0488	0.6953
C	9.0906	1.0733	0.7834	1.0806	0.9545
D	9.4598	1.1210	0.8249	0.8249	1.1210
E	8.6980	0.8745	1.3693	1.0007	0.6473
F	8.7158	0.8971	1.0488	1.0488	0.8971

D_1 and D_5 have the largest radii, and if there are two or more disks with equal and largest radius, then the distances between the disks are symmetric about the origin.

4.4. Condensation of a constellation of m disks into one disk

We study now the condensation of a constellation E of m hyperbolic disks with equal radii r into the case of one hyperbolic disk constellation with equal capacity, and compare the hyperbolic area and perimeter of the original and the new constellation. That

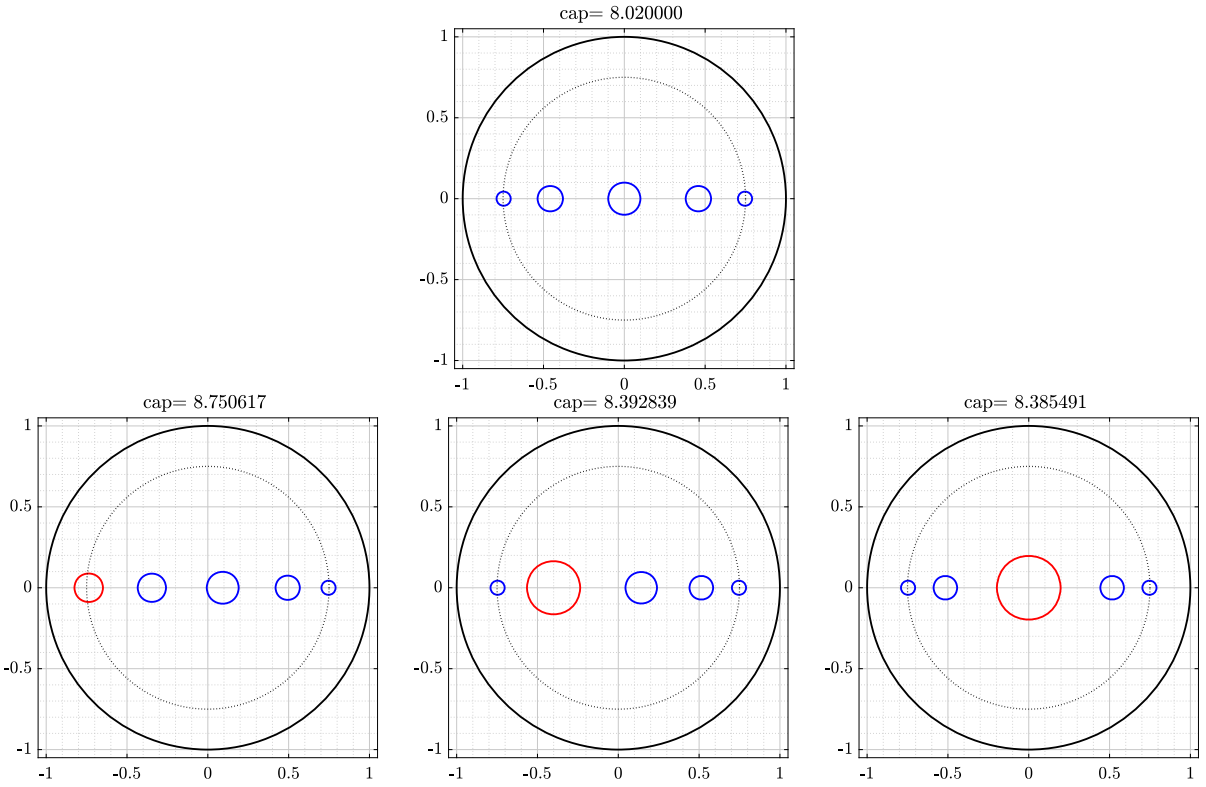

Fig. 16. First row: All disks have hyperbolic radius 0.2. Second row: One disk with hyperbolic radius 0.4 (red) and four disks with hyperbolic radii 0.2 (blue).

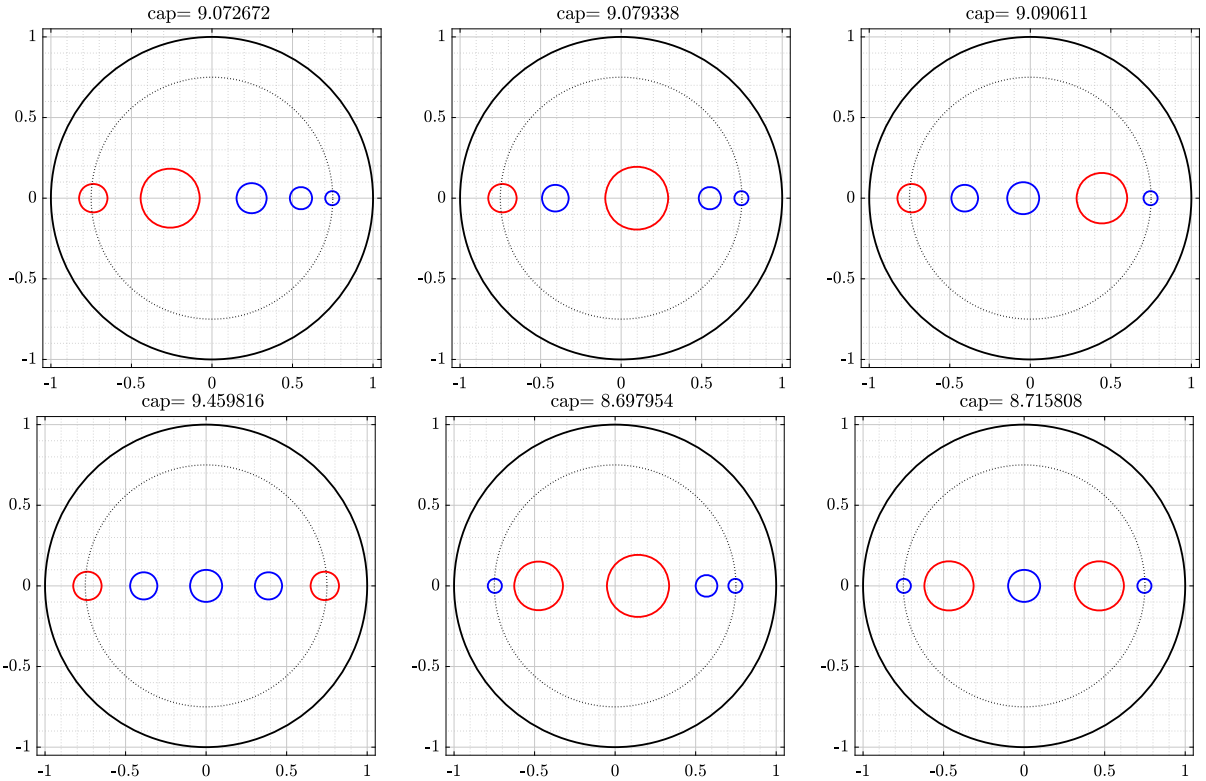

Fig. 17. Two disks have hyperbolic radius 0.4 (red) and three disks have hyperbolic radii 0.2 (blue).

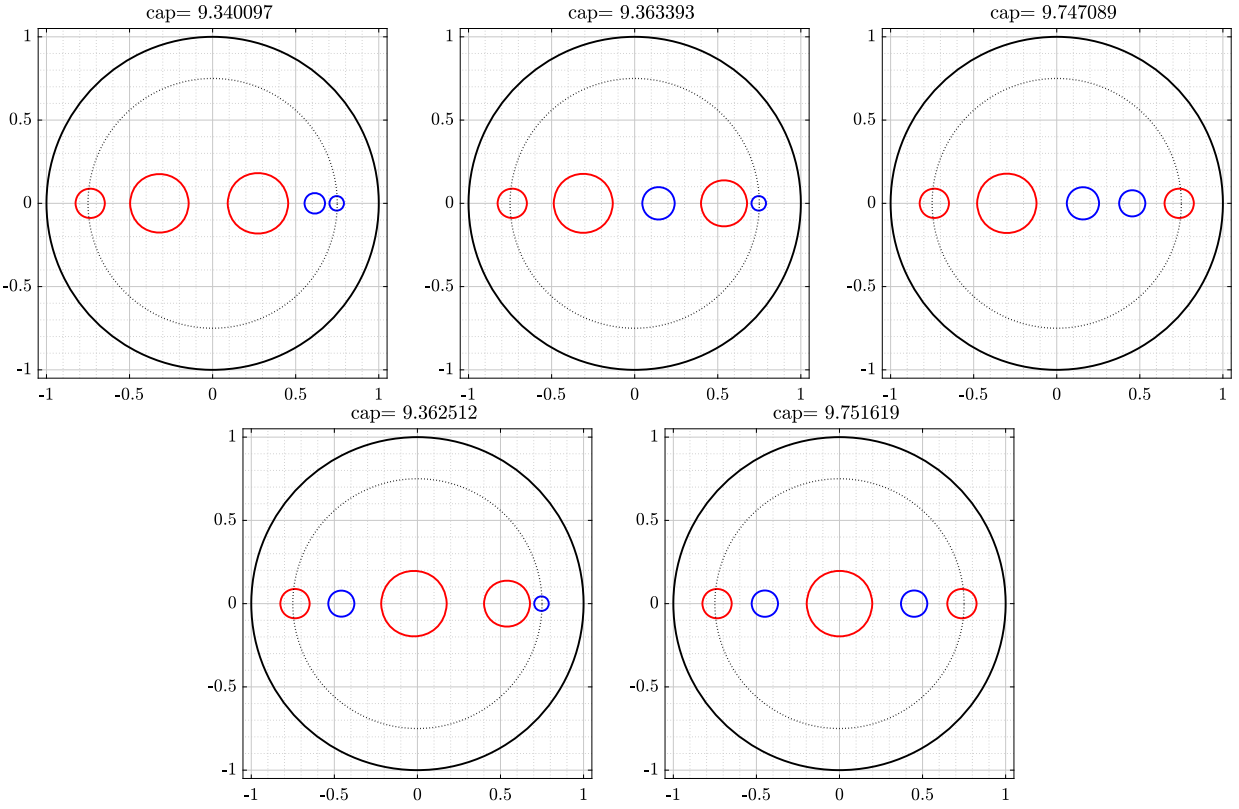

Fig. 18. Three disks have hyperbolic radius 0.4 (red) and two disks have hyperbolic radii 0.2 (blue).

Table 7
The hyperbolic distances between the centers of consecutive disks in Fig. 18.

Case	Capacity	$\rho(z_1,z_2)$	$\rho(z_2,z_3)$	$\rho(z_3,z_4)$	$\rho(z_4,z_5)$
A	9.3401	1.2558	1.2719	0.7477	0.5005
B	9.3634	1.2810	0.9565	0.9534	0.7010
C	9.7471	1.3014	0.9656	0.6684	0.9564
D	9.3625	0.9473	0.9550	1.2930	0.6966
E	9.7516	0.9693	0.9766	0.9766	0.9693

is, we assume that $E = \cup_{j=1}^{m} B_\rho(z_j, r)$ and we will find the value of R such that $\mathrm{cap}(\mathbb{B}^2, E) = \mathrm{cap}(\mathbb{B}^2, B_\rho(0, R))$. Recall first that the hyperbolic area and hyperbolic perimeter of a hyperbolic disk $B_\rho(z_j, r)$ are by [5, Thm 7.2.2, p. 132]

$$4\pi \,\mathrm{sh}^2\left(\frac{r}{2}\right) \quad \text{and} \quad 2\pi \,\mathrm{sh}\, r, \tag{4.1}$$

respectively.

Let $c = \mathrm{cap}(\mathbb{B}^2, E)$, which will be approximated numerically using the above discussed BIE method. Since, by 2.11,

$$\mathrm{cap}(\mathbb{B}^2, B_\rho(0, R)) = 2\pi / \log(1/\,\mathrm{th}(R/2)), \tag{4.2}$$

the value of the radius R of a single disk $B_\rho(0, R)$ with capacity equal to c satisfies

$$2\,\pi / \log(1/\mathrm{th}(R/2)) = c$$

and hence

$$R = 2\,\mathrm{arth}(e^{-2\pi/c}) = -\log\,\mathrm{th}(\pi/c). \tag{4.3}$$

As an example, we assume that $m = 6$ and the centers z_j of the hyperbolic disks $B_\rho(z_j, r)$ are given by

$$z_j = 0.75 e^{2\pi(j-1)\mathrm{i}/m}, \quad j = 1, 2, \ldots, m.$$

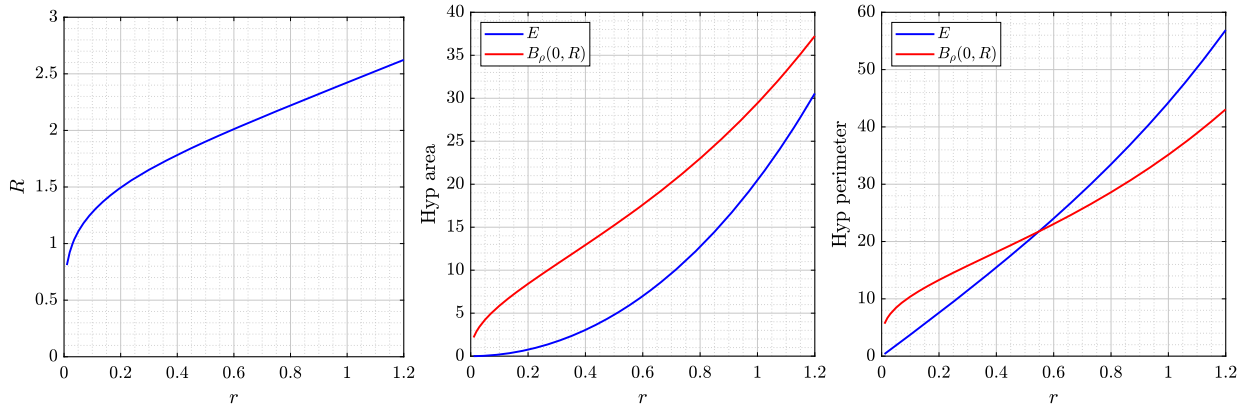

Fig. 19. Left: The values of R as a function of r such that $\operatorname{cap}(\mathbb{B}^2, B_\rho(0,R)) = \operatorname{cap}(\mathbb{B}^2, E)$ where $E = \cup_{j=1}^m B_\rho(z_j, r)$ for $m = 6$ and $z_j = 0.75e^{2\pi(j-1)\mathrm{i}/m}$, $j = 1, 2, \ldots, m$. Center and right: The hyperbolic area and perimeter of E and $B_\rho(0,R)$ as functions of r.

We compute the capacity $c = \operatorname{cap}(\mathbb{B}^2, E)$ using the above BIE method with $n = 2^{10}$. Then, we compute the values of R via (4.3). The computed values of R for $0.1 \le r \le 1.2$ are presented in Fig. 19. Then, by (4.1), the hyperbolic area and perimeter of the disk $B_\rho(0,R)$ are equal to $4\pi \operatorname{sh}^2\left(\frac{R}{2}\right)$ and $2\pi \operatorname{sh} R$, respectively. Note that the hyperbolic area and perimeter of E are given by

$$4m\pi \operatorname{sh}^2\left(\frac{r}{2}\right) \quad \text{and} \quad 2m\pi \operatorname{sh} r,$$

respectively. The hyperbolic area and perimeter of E and $B_\rho(0,R)$ are presented in Fig. 19. The obtained results show that the hyperbolic area of the single disk $B_\rho(0,R)$ is always greater than the sum of the hyperbolic area of the six disks. However, the hyperbolic perimeter of the single disk $B_\rho(0,R)$ is greater than the sum of the hyperbolic perimeter of the six disks for small values of r. For large values of r, the perimeter of the six disks is greater than the perimeter of the single disk.

5. Numerical experiments: slit constellations

In this section the elements of the constellations are hyperbolic segments of constant length. The experiments follow the same pattern as those above, however, the constraints on configurations are more restrictive. Again, we start with two segments and then increase complexity by adding more segments to the constellations.

5.1. Constellation of two hyperbolic segments

We assume that the constellation E is the union of two non-overlapping hyperbolic symmetric collinear segments I_1 an I_2 with equal hyperbolic length ℓ such that the centers of these segments are $\pm xe^{\mathrm{i}\theta}$ on the line $\arg(z) = \theta \in [0, \pi)$ where

$$\operatorname{th}\frac{\ell}{4} < x < 1,$$

and hence $\rho\left(-xe^{\mathrm{i}\theta}, xe^{\mathrm{i}\theta}\right) > \ell$. The values of $\operatorname{cap}(\mathbb{B}^2, E)$ vs. x are shown in Fig. 20 (left) for $\theta = 0$, $\ell = 1$ and in Fig. 20 (right) for $\theta = 0$, $\ell = 2$. Note that

$$\operatorname{cap}(\mathbb{B}^2, I_i) = \frac{2\pi}{\mu(\operatorname{th}(\ell/2))}, \quad i = 1, 2,$$

and hence

$$\operatorname{cap}(\mathbb{B}^2, I_1) + \operatorname{cap}(\mathbb{B}^2, I_2) = 2\operatorname{cap}(\mathbb{B}^2, I_1) = \frac{4\pi}{\mu(\operatorname{th}(\ell/2))}$$

is an upper bound for $\operatorname{cap}(\mathbb{B}^2, E)$. The values of this upper bound are shown in Fig. 20 as "dotted line."

The two segments merge into one segment $\hat{I}$ of hyperbolic length 2ℓ when $x = \operatorname{th}\frac{\ell}{4}$. Thus

$$\operatorname{cap}(\mathbb{B}^2, \hat{I}) = \frac{2\pi}{\mu(\operatorname{th}(\ell))}$$

is a lower bound for $\operatorname{cap}(\mathbb{B}^2, E)$. The values of $\operatorname{cap}(\mathbb{B}^2, \hat{I})$ are shown in Fig. 20 as "dashed line."

Fig. 20 shows that $\operatorname{cap}(\mathbb{B}^2, E) \to 4\pi/\mu(\operatorname{th}(\ell/2))$ as $x \to 1$ and $\operatorname{cap}(\mathbb{B}^2, E) \to 2\pi/\mu(\operatorname{th}(\ell))$ as $x \to \operatorname{th}(\ell/4)$.

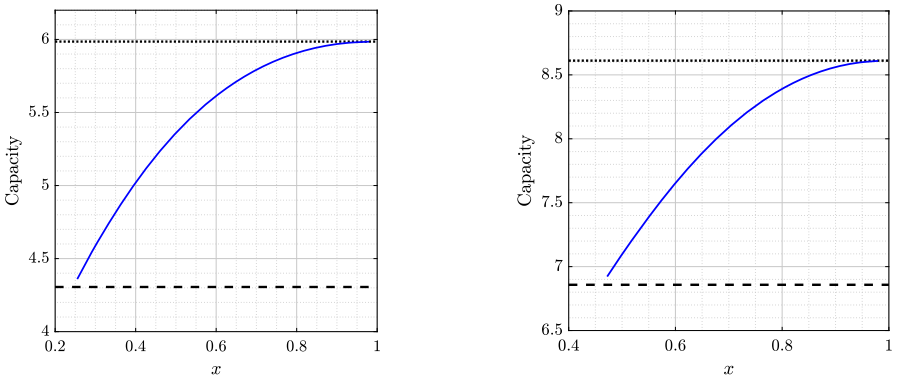

Fig. 20. Two hyperbolic segments with hyperbolic length $\ell = 1$ (left) $\ell = 2$ (right). The centers of these segments are $\pm xe^{i\theta}$ for $\theta = 0$.

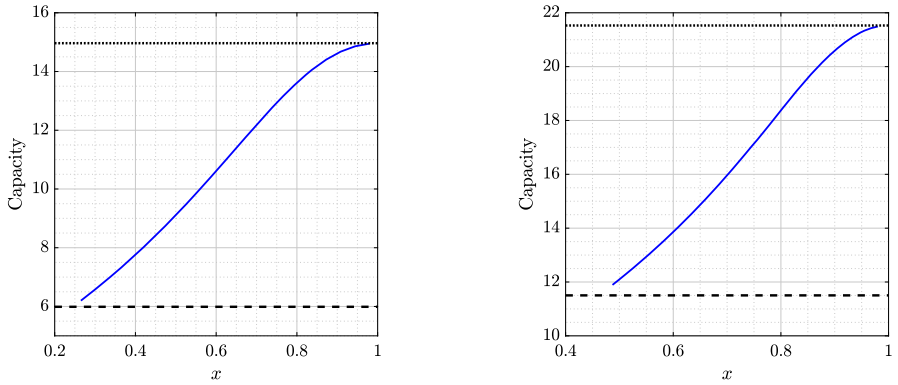

Fig. 21. Five radial hyperbolic segments with hyperbolic length $\ell = 1$ (left) $\ell = 2$ (right). The centers of these segments are $xe^{2k\pi i/5}$, $k = 1, \ldots, 5$.

5.2. Constellation of five radial hyperbolic segments with constant angle of separation

Next we let E be the union of five non-overlapping hyperbolic segments, $I_1, \ldots, I_5$, with equal hyperbolic length ℓ such that the center of the segment I_k is $xe^{2k\pi i/5}$ where

$$\operatorname{th}\frac{\ell}{4} < x < 1.$$

The computed approximate values of $\operatorname{cap}(\mathbb{B}^2, E)$ vs. x are shown in Fig. 21 (left) for $\ell = 1$ and in Fig. 21 (right) for $\ell = 2$. Note that the five segments merge into one connected set $\hat{I}$ when $x = \operatorname{th}\frac{\ell}{4}$. Thus, using the same approach used in [29, Lemma 6.8], we can prove that

$$\operatorname{cap}(\mathbb{B}^2, \hat{I}) = \frac{10\pi}{\mu(\operatorname{th}^5(\ell/2))}$$

which is a lower bound for $\operatorname{cap}(\mathbb{B}^2, E)$. The values of $\operatorname{cap}(\mathbb{B}^2, \hat{I})$ are shown in Fig. 21 as "dashed line." As in the previous example,

$$\sum_{k=1}^{5} \operatorname{cap}(\mathbb{B}^2, I_k) = 5 \operatorname{cap}(\mathbb{B}^2, I_1) = \frac{10\pi}{\mu(\operatorname{th}(\ell/2))}$$

is an upper bound for $\operatorname{cap}(\mathbb{B}^2, E)$. The values of this upper bound are shown in Fig. 21 as "dotted line."

For numerical computing of the capacity $\operatorname{cap}(\mathbb{B}^2, \hat{I})$, we use the *hp*-FEM where the absolute error in the computed capacity is 2×10^{-12} and 8×10^{-12} for the short and long segments, respectively. Plots of the potential function for the capacity $\operatorname{cap}(\mathbb{B}^2, E)$ are presented in Fig. 22. See Fig. 23.

5.3. Constellation of six hyperbolic segments constrained to a disk

Analogously to the case with disks, we consider the positions of six hyperbolic segments that maximize the capacity $\operatorname{cap}(\mathbb{B}^2, E)$ under the constraint that the hyperbolic centers of these disks are in the Euclidean disk $|z| \le R$ (we assume in the examples below that $R = 0.75$). The segments are numbered E_1 to E_6 in counterclockwise orientation. We denote the center of the disk E_j by z_j, $j = 1, \ldots, 6$. Without loss of generality, we assume that the center z_1 of the segment E_1 is on the positive real axis.

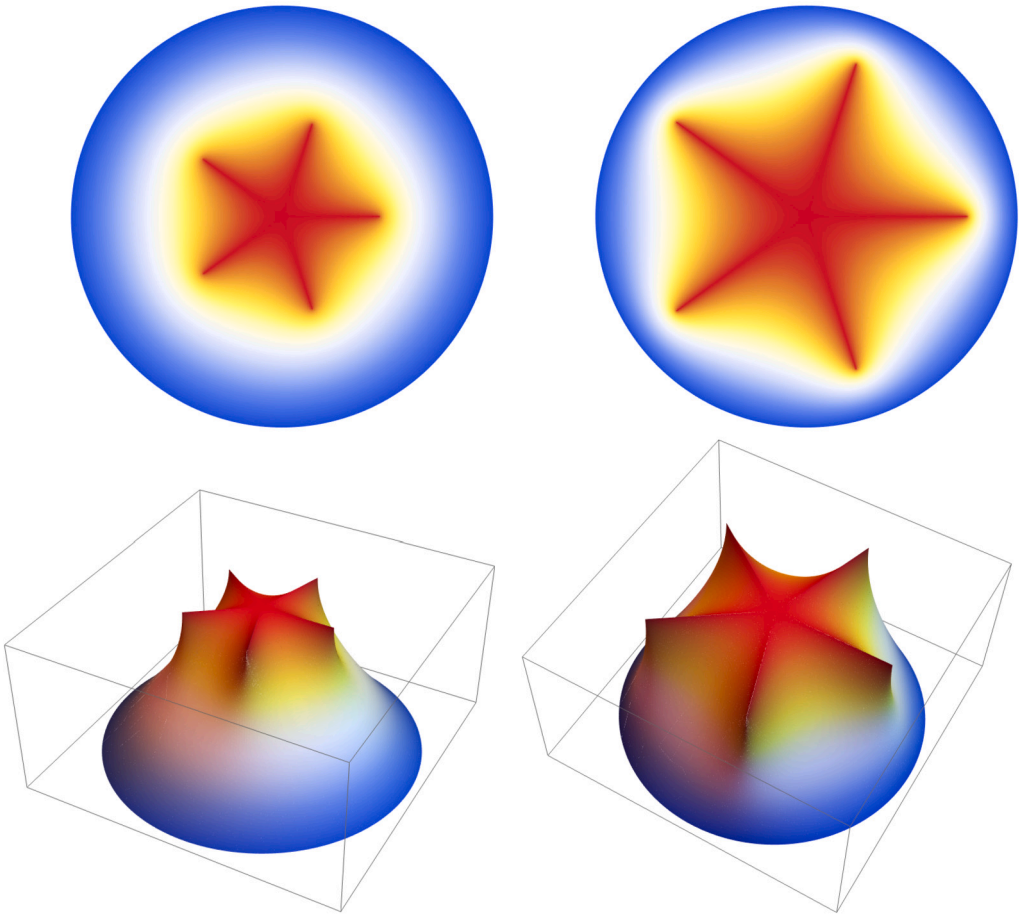

Fig. 22. Five radial hyperbolic segments. Surface plots of the potentials in the lower limit cases when all segments meet at the origin.

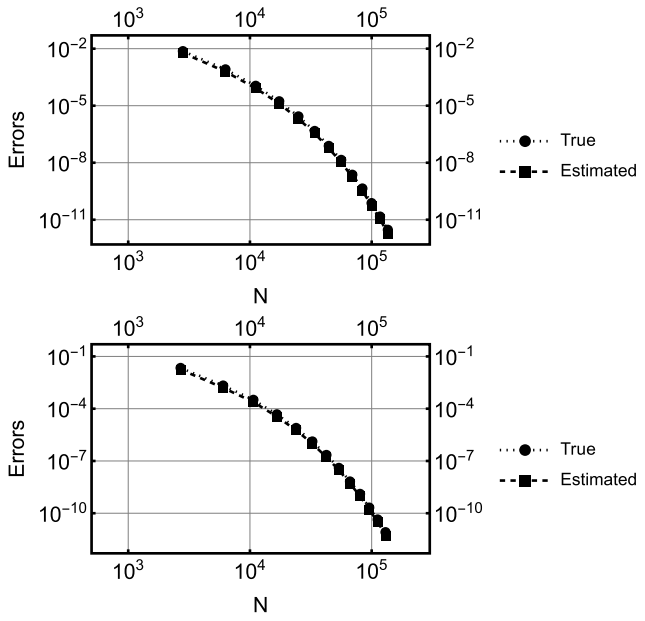

Fig. 23. Five radial hyperbolic segments. Error convergence: (Top) Short segments, (Bottom) Long segments. Both exact and estimated errors are shown in loglog-plots, N is the number of degrees of freedom.

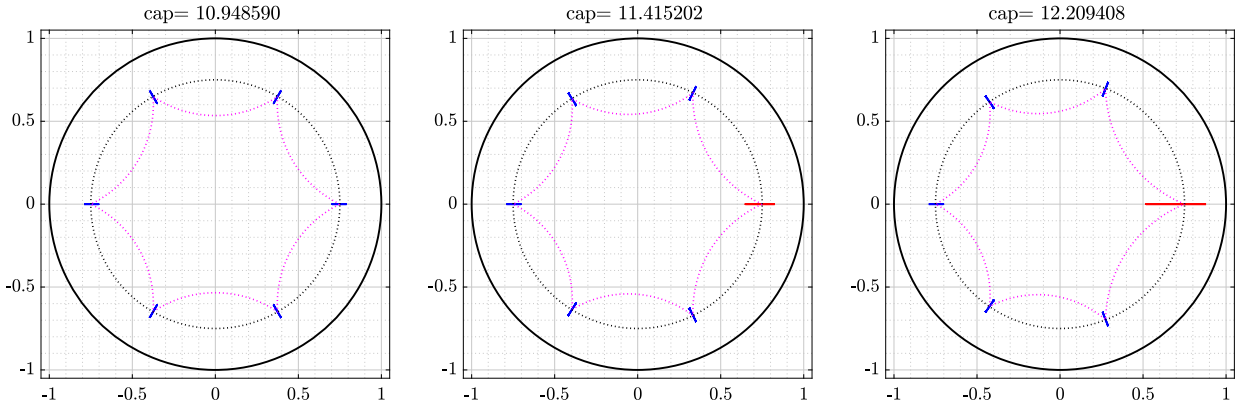

Fig. 24. Segment E_1 has hyperbolic length 0.4 (left), 0.8 (center), and 1.6 (right). Segments E_2 through E_6 have hyperbolic length 0.4.

Table 8
The hyperbolic distance between the centers of consecutive segments in Fig. 24.

Case	Capacity	$\rho(z_1,z_2)$	$\rho(z_2,z_3)$	$\rho(z_3,z_4)$	$\rho(z_4,z_5)$	$\rho(z_5,z_6)$	$\rho(z_6,z_1)$
A	10.9486	2.6161	2.6161	2.6161	2.6161	2.6161	2.6161
B	11.4152	2.7080	2.5705	2.5655	2.5655	2.5705	2.7080
C	12.2094	2.8236	2.5089	2.4931	2.4931	2.5089	2.8236

Table 9
The hyperbolic distances between the centers of consecutive segments in Fig. 25.

Case	Capacity	$\rho(z_1,z_2)$	$\rho(z_2,z_3)$	$\rho(z_3,z_4)$	$\rho(z_4,z_5)$
A	6.7011	0.9293	1.0166	1.0166	0.9293
B	7.0648	1.1379	0.9521	0.9439	0.8579
C	6.8703	1.0317	1.1313	0.9071	0.8218
D	6.8688	0.8222	1.1237	1.1237	0.8222

First we assume that all six segments have equal hyperbolic length = 0.4. The positions of these six segments that maximize the capacity $\mathrm{cap}(\mathbb{B}^2, E)$ are on the Euclidean circle $|z| = R$ and such the hyperbolic distances between the centers of any two adjacent segments are equal (see Fig. 24 (left) and Table 8). When we change the hyperbolic length of one of these segments to be 0.8 (see Fig. 24 (center)) or 1.6 (see Fig. 24 (right)), then the centers of the other segments are moved away from the larger segment (see Table 8).

5.4. *Constellation of five hyperbolic segments constrained to the real line*

In the final experiment we consider the positions of five hyperbolic segments that maximize the capacity $\mathrm{cap}(\mathbb{B}^2, E)$ under the constraint that the hyperbolic centers of these slits are in the interval $[-R, R]$ (we assume in the examples below that $R = 0.75$). The segments are numbered $(E_1, \ldots, E_5)$ from left to right.

First all five segments are set to have equal hyperbolic length = 0.4. The positions of these five segments that maximize the capacity $\mathrm{cap}(\mathbb{B}^2, E)$ are shown in Fig. 25 and the hyperbolic distance between the centers of any two adjacent segments is presented in Table 9. Then we change the hyperbolic length of one of these segments to be 0.8. The obtained results are presented in Fig. 25 and Table 9.

In all cases the results computed with BIE and FEM agree within the prescribed tolerance.

5.4.1. *On computational costs*

Optimization with the object function obtained by means of PDE solution is inherently expensive. In Table 10 performance data on the six disks maximization problem shown in Fig. 1 is presented. In all cases the interior-point tolerance is the same, $\epsilon = 10^{-6}$, and within the *hp*-FEM simulations, meshing is performed with the same discretization control in every evaluation. Not surprisingly, the overall conclusions are very similar to those drawn in our previous work [16], where minimization was considered. Comparison of the two methods is only qualitative, since both underlying hardware and the interior-point implementations are different.

The two implementations have very different requirements per iteration step. It is very likely that this is due to the fact that the numerical differentiation algorithm of Matlab is different from the one of Mathematica. Observe that the number of iteration steps becomes comparable once the *hp*-solutions are sufficiently accurate, yet the number of evaluations is not. The average time for one evaluation in BIE is four to five times faster than one evaluation in *hp*-FEM. Matlab and Mathematica results have been computed on

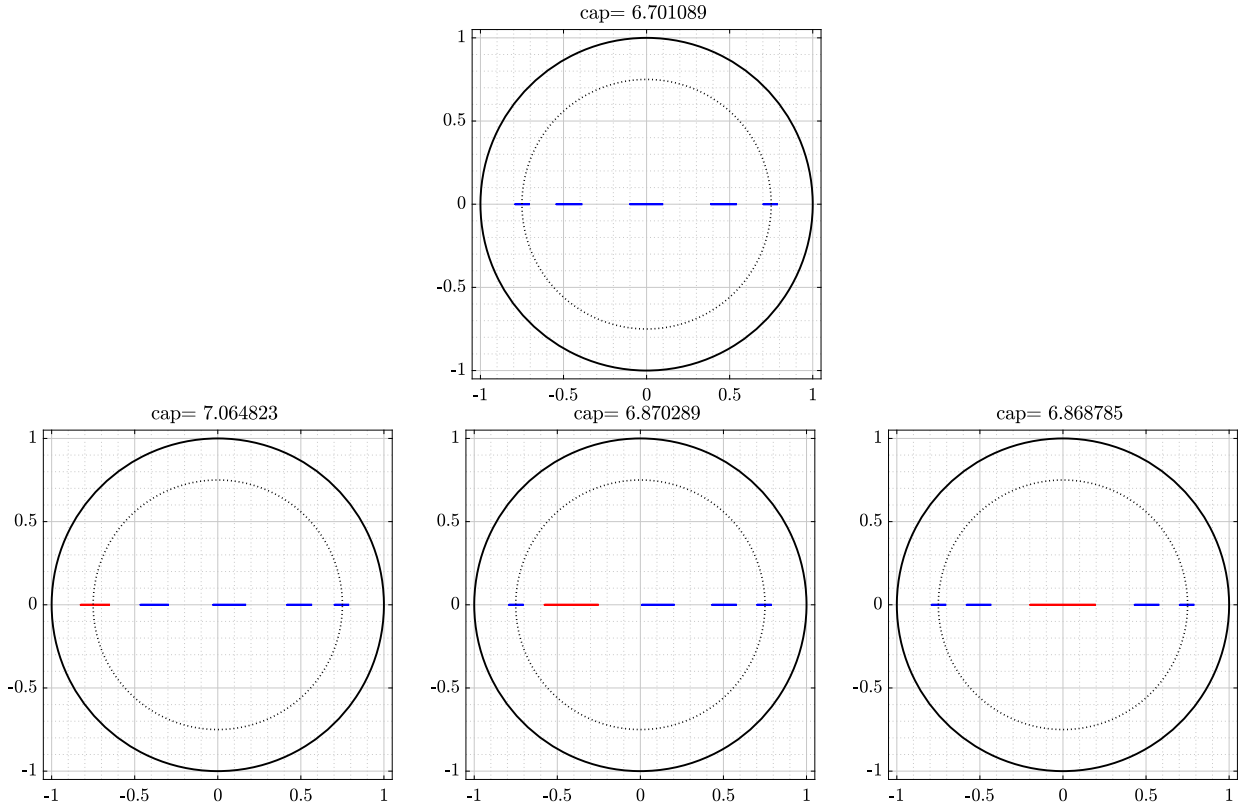

Fig. 25. First row: All segments have hyperbolic length 0.4. Second row: One segment with hyperbolic length 0.8 (red) and four segments with hyperbolic length 0.4 (blue).

Table 10
Solution times for the maximization process for the six hyperbolic disks in Fig. 1. Number of steps is number of iterations in the interior-point algorithm. Number of evaluations is the total number of solves performed during the maximization.

Method	Discretization	Time	# of steps	# of evaluations
BIE	$n = 2^6$	162.5	16	204
	$n = 2^8$	274.7	17	216
	$n = 2^{10}$	637.8	22	286
hp-FEM	$p = 4$	21749.2	144	23706
	$p = 6$	5132.6	24	3704
	$p = 8$	2170.9	6	1050

Lenovo ThinkPad with Intel Core i9-12900HX, 2300 Mhz, 16 Core(s), 24 Logical Processors and 64 GB RAM, and Apple Silicon Mac mini M2 Pro 32GB (2023), respectively.

In short, for optimal performance, the individual solutions must be accurate enough so that the error induced by numerical approximation of the gradients and Hessians is balanced with other sources of error. For BIE, the problem is practically fully resolved already at $n = 2^6$, whereas for the *hp*-FEM it appears that the same mesh with $p = 4$ is not adequate in comparison with the one at $p = 8$. Even though the time spent in one individual iteration step is doubled, the overall time for $p = 8$ is significantly lower.

It is clear from Table 10 that obtaining the positions of the inner disks that maximize the capacity requires computing the capacity for hundreds of times which can be computed accurately using the two proposed methods. To illustrate the accuracy and the computational cost of the two methods for each evaluation of the capacity, we discuss in details the computation of the capacity of the initial domain in Fig. 1 (left) and the computed domain with maximum capacity in Fig. 1 (right). For both domains, the value of the capacity is computed with $n = 2^{13}$ to obtain $\mathrm{cap}(\mathbb{B}^2, E) = 7.288440106260681$ for the domain in Fig. 1 (left) and $\mathrm{cap}(\mathbb{B}^2, E) = 13.757382935965428$ for the domain in Fig. 1 (right). These two computed values are considered as the reference values and used to estimate the error in the values of $\mathrm{cap}(\mathbb{B}^2, E)$ computed by the two numerical methods. The computed error for the BIE method as a function of n is presented in Fig. 26 (left) where Case I is the domain in Fig. 1 (left) and Case II is the domain in Fig. 1 (right). Similar convergence graphs are shown for the *hp*-FEM in Fig. 27. For the cases with smooth boundaries both methods

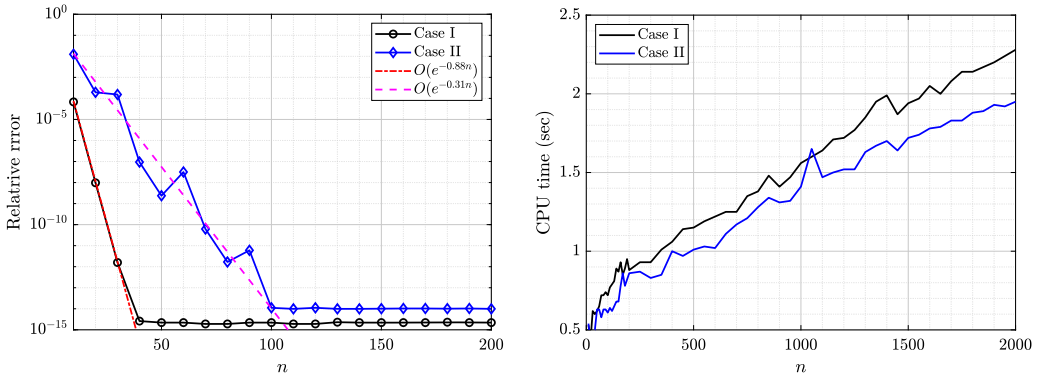

Fig. 26. Left: The errors in the computed values of $\mathrm{cap}(\mathbb{B}^2, E)$ using the BIE method as functions of n for both domains in Fig. 1. Right: Run time in seconds as a function of n required to compute $\mathrm{cap}(\mathbb{B}^2, E)$ using the BIE method.

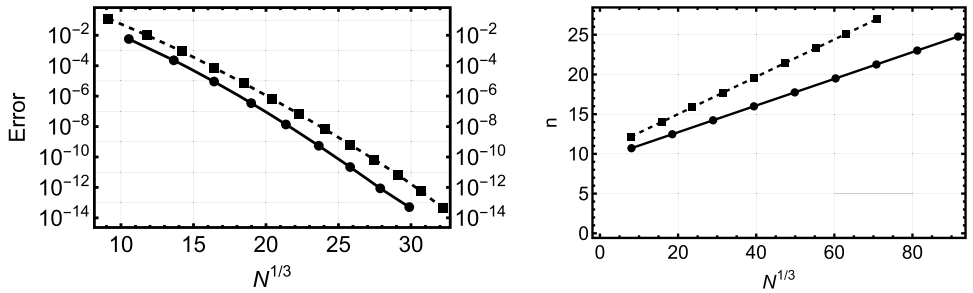

Fig. 27. Left: The errors in the computed values of $\mathrm{cap}(\mathbb{B}^2, E)$ using the hp-FEM as functions of $N^{1/3}$ for both domains in Fig. 1. Right: Comparison of $N^{1/3}$ (hp-FEM) vs n (BIE). The dashed line refers to the maximal constellation.

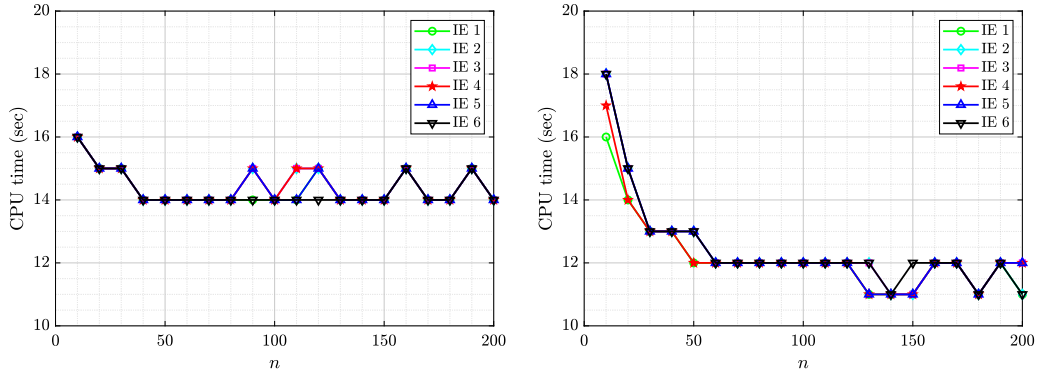

Fig. 28. The number of GMRES iterations as a function of n required to solve the $m = 6$ integral equations for the two domains in Fig. 1.

convergence exponentially and we conclude that the complexity comparison can be reduced to $n \sim N^{1/3}$, where n is the number of quadrature points in BIE method and N is the number of degrees of freedom in FEM. Notice that this rate for FEM is the optimal one given in Theorem 3.1.

Computing the capacity $\mathrm{cap}(\mathbb{B}^2, E)$ using the BIE method requires solving the boundary integral equation (3.7) for m times. The computation of the right-hand side of the integral equation requires $O((m+1)n \ln n)$ operations and each iteration of the GMRES method requires $O((m+1)n)$ operations [26]. Thus, solving the integral equation requires $O((m+1)n \ln n)$ operations and hence computing the capacity $\mathrm{cap}(\mathbb{B}^2, E)$ requires, approximately, $O((m+1)^2 n \ln n)$ operations. To corroborate this, we present in Fig. 26 (right) a plot of the CPU time (in seconds) as a function of n required to compute the capacity of the two domains in Fig. 1. It is clear from these graphs that the CPU time depends almost linearly on n. We also provide in Fig. 28 the number of GMRES iterations required to solve the $m = 6$ integral equations for the two domains. These graphs show that the number of GMRES iterations is almost independent of n. On one hand, the number of iterations for the domain in Fig. 1 (left) is less than the number of iterations for the domain in Fig. 1 (right) since the disks on the right are well-separated compared to the disks on the left. This implies that the CPU time required to compute the capacity of the domain on the right is less than the CPU time for the domain on the left. On the other

hand, it is clear from Fig. 26 that the order of convergence for the domain on the left is better than the order of convergence for the domain on the right. A possible reason for that is the inner disks for the domain on the right are closer to the external boundary compared to the domain on the left. A detailed analysis of the order of convergence for the above BIE method is beyond the scope of the current paper and will be a subject of future work.

The computational complexity of the hp-FEM is comprehensively documented in the references by Schwab [33] and Szabo and Babuška [35]. In contrast to the standard h-version the numerical integration of the inner products typically amounts to one half of the solution times.

Remark 5.1. In comparison with similar minimization problems in [16], we observe that the constrained maximization problems are less resource intensive in terms of iteration steps and runtimes. This is more notable in the BIE results. Our interpretation is that in maximization the boundary components are relatively faraway from each other and hence high accuracy results can be obtained for moderate values of n and few number of iterations.

6. Conclusions

Maximizing the conformal capacity of a constellation is opposite to minimizing studied in [16]. In [16] the main result was that the disks of the constellation group together in the local minima cases. Here we have shown that in the case of maximization the expected natural dispersion phenomenon occurs: the disks move as close to the unit circle as the constraints permit and, at the same time, the disks keep as far away from each other as possible. Replacing disks by other simple geometric objects also seems possible as our experiments with radial and rectilinear segments show.

A mathematical proof of the extremal cases we found in the experiments is missing. However, based on the numerical experiments we can predict the maximal capacities of all constellations exhibiting sectorial symmetry. In this case the constellation capacity is additive, equal to the sum of the capacities of the sectors or compartments. This was studied in [6] and [21] from another point of view and similar conclusions obtained.

The study of this topic seems to offer many opportunities for later research. For example, one could study the above problems replacing the unit disk by some other domain, e.g. by a polygonal domain. Also one could investigate similar problems for other capacities such as the logarithmic and analytic capacities.

Acknowledgements

The authors would like to thank two anonymous reviewers for their valuable comments and suggestions which greatly improved the presentation of this paper.

Appendix A. Code availability

In the interest of reproducibility, the codes for our computations are available through the link https://github.com/mmsnasser/maxcap.

Data availability

No data was used for the research described in the article.

References

[1] M. Abramowitz, I.A. Stegun, Handbook of Mathematical Functions, 10th ed., Dover, New York, 1972.
[2] K.E. Atkinson, The Numerical Solution of Integral Equations of the Second Kind, Cambridge University Press, Cambridge, 1997.
[3] I. Babuška, B. Guo, Regularity of the solutions of elliptic problems with piecewise analytical data, parts I and II, SIAM J. Math. Anal. 19 (1988) 172–203, SIAM J. Math. Anal. 20 (1989) 763–781.
[4] A. Baernstein, Symmetrization in Analysis, With David Drasin and Richard S. Laugesen. With a foreword by Walter Hayman, New Mathematical Monographs, vol. 36, Cambridge University Press, Cambridge, 2019.
[5] A.F. Beardon, The Geometry of Discrete Groups, Springer-Verlag, New York, 1983.
[6] D. Betsakos, A. Solynin, M. Vuorinen, Conformal capacity of hedgehogs, Conform. Geom. Dyn. 27 (2023) 55–97.
[7] S.V. Borodachov, D.P. Hardin, E.B. Saff, Discrete Energy on Rectifiable Sets, Springer Monographs in Mathematics, Springer, New York, 2019.
[8] D.G. Crowdy, Solving Problems in Multiply Connected Domains, SIAM, 2020.
[9] D.G. Crowdy, E.H. Kropf, C.C. Green, M.M.S. Nasser, The Schottky-Klein prime function: a theoretical and computational tool for applications, IMA J. Appl. Math. 81 (2016) 589–628.
[10] J.P.K. Doye, D.J. Wales, Magic numbers and growth sequences of small face-centered-cubic and decahedral clusters, J. Chem. Phys. 102 (22) (1995) 9673–9688.
[11] P.D. Dragnev, B. Fuglede, D.P. Hardin, E.B. Saff, N. Zorii, Constrained minimum Riesz energy problems for a condenser with intersecting plates, J. Anal. Math. 140 (2020) 117–159.
[12] V.N. Dubinin, Condenser Capacities and Symmetrization in Geometric Function Theory, Birkhäuser, 2014.
[13] F.W. Gehring, Inequalities for condensers, hyperbolic capacity, and extremal lengths, Mich. Math. J. 18 (1971) 1–20.
[14] V.M. Goldshtein, Yu.G. Reshetnyak, Quasiconformal Mappings and Sobolev Spaces, Kluwer Academic Publishers Group, Dordrecht, 1990.
[15] L. Greengard, Z. Gimbutas, FMMLIB2D: a MATLAB toolbox for fast multipole method in two dimensions, version 1.2, www.cims.nyu.edu/cmcl/fmm2dlib/fmm2dlib.html, 2019. (Accessed 6 November 2020).

[16] H. Hakula, M.M.S. Nasser, M. Vuorinen, Mobile disks in hyperbolic space and minimization of conformal capacity, Electron. Trans. Numer. Anal. 60 (2024) 1–19.
[17] H. Hakula, M. Neilan, J. Ovall, A posteriori estimates using auxiliary subspace techniques, J. Sci. Comput. 72 (1) (2017) 97–127.
[18] H. Hakula, T. Tuominen, Mathematica implementation of the high order finite element method applied to eigenproblems, Computing 1 (95) (2013) 277–301.
[19] P. Hariri, R. Klén, M. Vuorinen, Conformally Invariant Metrics and Quasiconformal Mappings, Springer Monographs in Mathematics, Springer, Berlin, 2020.
[20] J. Heinonen, T. Kilpeläinen, O. Martio, Nonlinear Potential Theory of Degenerate Elliptic Equations, Dover Publications, New York, 2006.
[21] E.M. Kalmoun, M.M.S. Nasser, M. Vuorinen, Numerical computation of a preimage domain for an infinite strip with rectilinear slits, Adv. Comput. Math. 49 (2023) 5.
[22] P. Koebe, Abhandlungen zur Theorie der konformen Abbildung, IV. Abbildung mehrfach zusammenhängender schlichter Bereiche auf Schlitzbe-reiche, Acta Math. 41 (1918) 305–344.
[23] MATLAB, 9.12 (R2022a), The MathWorks Inc., Natick, Massachusetts, 2022.
[24] H. Miyoshi, D.G. Crowdy, Estimating conformal capacity using asymptotic matching, IMA J. Appl. Math. 88 (2023) 472–497.
[25] M.M.S. Nasser, Numerical conformal mapping of multiply connected regions onto the second, third and fourth categories of Koebe's canonical slit domains, J. Math. Anal. Appl. 382 (2011) 47–56.
[26] M.M.S. Nasser, Fast solution of boundary integral equations with the generalized Neumann kernel, Electron. Trans. Numer. Anal. 44 (2015) 189–229.
[27] M.M.S. Nasser, C.C. Green, A fast numerical method for ideal fluid flow in domains with multiple stirrers, Nonlinearity 31 (2018) 815–837.
[28] M.M.S. Nasser, M. Vuorinen, Numerical computation of the capacity of generalized condensers, J. Comput. Appl. Math. 377 (2020) 112865.
[29] M.M.S. Nasser, M. Vuorinen, Isoperimetric properties of condenser capacity, J. Math. Anal. Appl. 499 (2021) 125050.
[30] J. Nocedal, S. Wright, Numerical Optimization, Springer, New York, NY, 2006.
[31] N. Papamichael, Numerical conformal mapping onto a rectangle with applications to the solution of Laplacian problems, J. Comput. Appl. Math. 28 (1989) 63–83.
[32] G. Pólya, G. Szegö, Isoperimetric Inequalities in Mathematical Physics, Annals of Mathematics Studies, vol. 27, Princeton University Press, Princeton, N.J., 1951.
[33] Ch. Schwab, p- and hp-Finite Element Methods, Oxford University Press, 1998.
[34] A.Yu. Solynin, V.A. Zalgaller, An isoperimetric inequality for logarithmic capacity of polygons, Ann. Math. (2) 159 (1) (2004) 277–303.
[35] B. Szabo, I. Babuška, Finite Element Analysis, Wiley, 1991.
[36] L.N. Trefethen, J.A.C. Weideman, The exponentially convergent trapezoidal rule, SIAM Rev. 56 (2014) 385–458.
[37] D.J. Wales, J.P.K. Doye, Global optimization by basin-hopping and the lowest energy structures of Lennard-Jones clusters up to $N = 110$, J. Phys. Chem. A 101 (28) (1997) 5111–5116.
[38] Wolfram Research, Inc., Mathematica, Version 14.0, Champaign, IL, 2024.